

3. Cloud Patterns

Cloud patterns are represented in visual imagery in relation to proximity to atmospheric flow, as well as the distribution and vertical stability of temperature and water vapor. Analysis of individual patterns is crucial in understanding 3-D atmospheric structures.

3.1. Ci Streaks

Long thin Ci streaks from jet streams and other sources are observed in the upper atmosphere with anticyclonic curvature corresponding to upper-trough conditions. Cloud areas also develop further when lower clouds are enhanced. Ci streaks (indicated with arrows) are seen over the Bohai Sea in Fig. 3-1-1 and along the jet in Fig. 3-1-2.

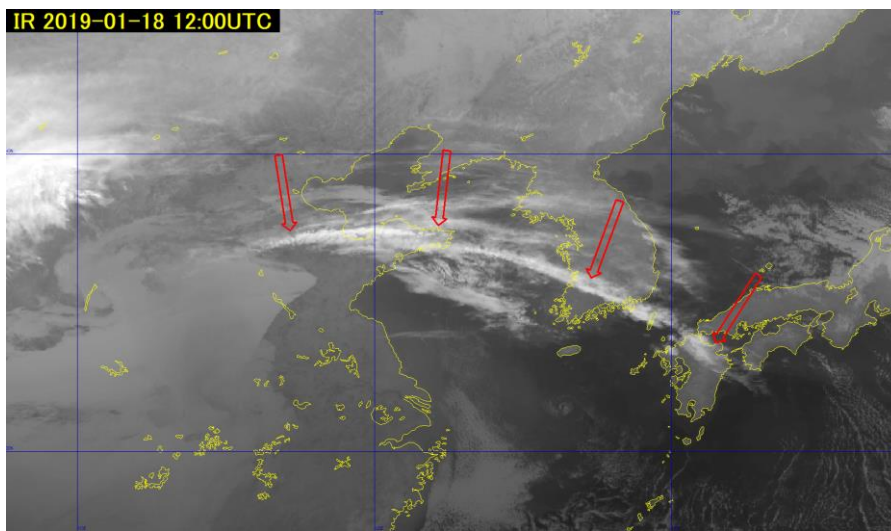


Fig. 3-1-1. B13 Infrared image of Ci streaks for 00:00 UTC on 13 October 2016

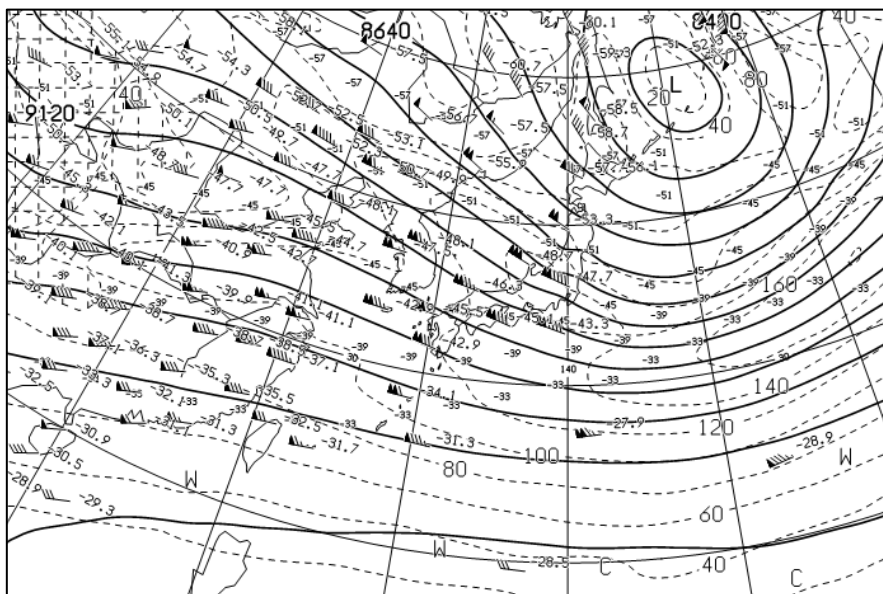


Fig. 3-1-2. Image for 00:00 UTC on 13 October 2016, 200 hPa isohypse

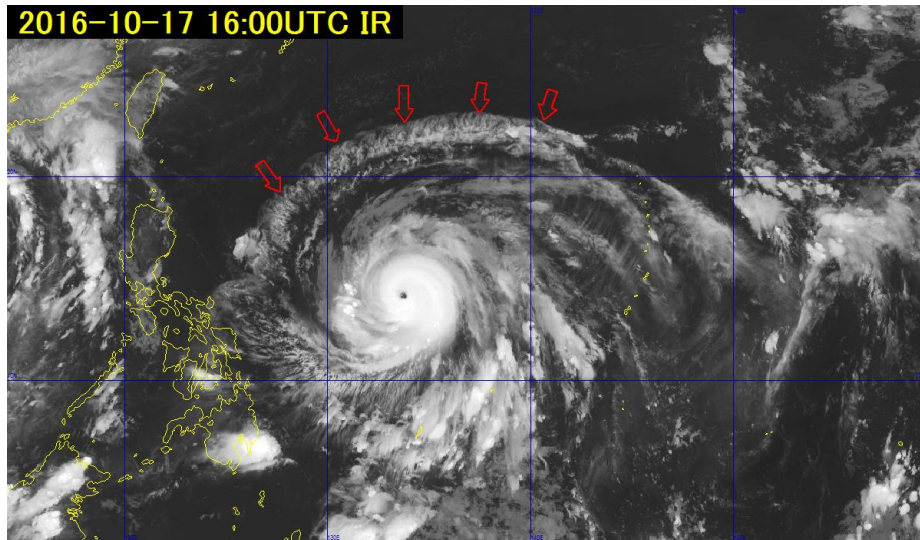


Fig. 3-2-3. B13 infrared image for 16:00 UTC on 17 October 2106

3.3. Orographic Ci Clouds

The stagnant orographic high clouds observed on the leeward side of mountain ranges appear white in infrared imagery, with a rim on the windward side parallel to the range and elongated to the leeward side. They are easily identifiable in footage, as the rim on the windward side hardly moves. They are observed in association with roughly stable stratification between mountain ranges and the upper tropopause with roughly steady wind speeds (Kobana, 1981), causing a transfer of mountain-associated waves to the upper layer in the updraft region via wave motion with significant upper-layer humidity. The waves remain stationary as long as the synoptic field remains unchanged, manifesting as stagnant upper clouds.

Figure 3-3-1 shows B13 infrared image from Himawari-8, with orographic Ci occurring leeward east of the Ou mountains (arrow indication), and Fig. 3-3-2 shows B03 visible image for the same time period. The pictures show transparent cirrus cloud in the upper layer.

Figure 3-3-3 shows numerical prediction grid point values from JMA's mesoscale numerical weather prediction model (MSM) around Sendai at 00:00 UTC on the same day. Upper cloud with humidity is seen at around 250 – 300 hPa, with strong vertical western wind distribution in the upper troposphere creating stable stratification.

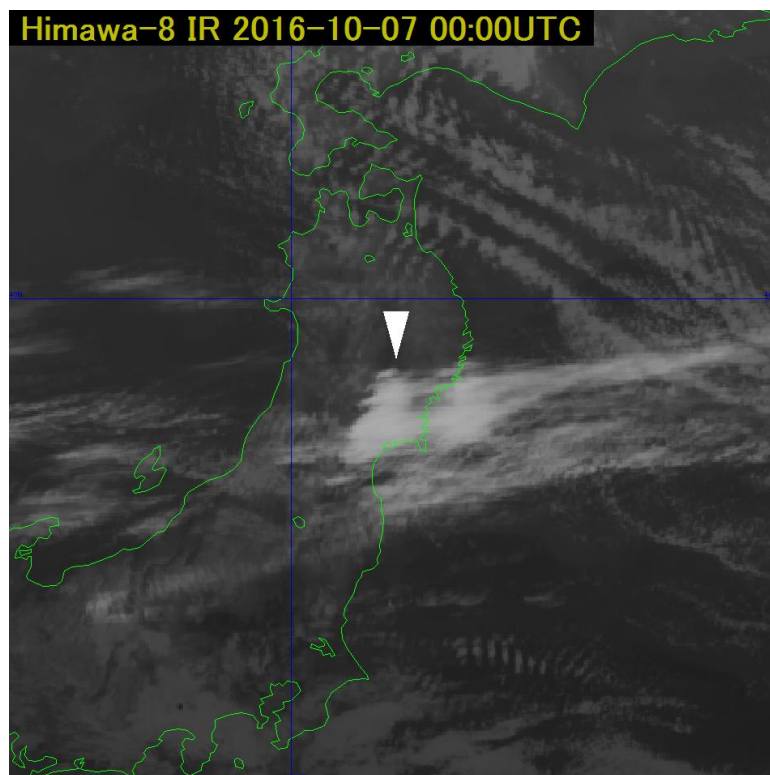


Fig. 3-3-1. B13 infrared image for 00:00 UTC on 7 October 2016

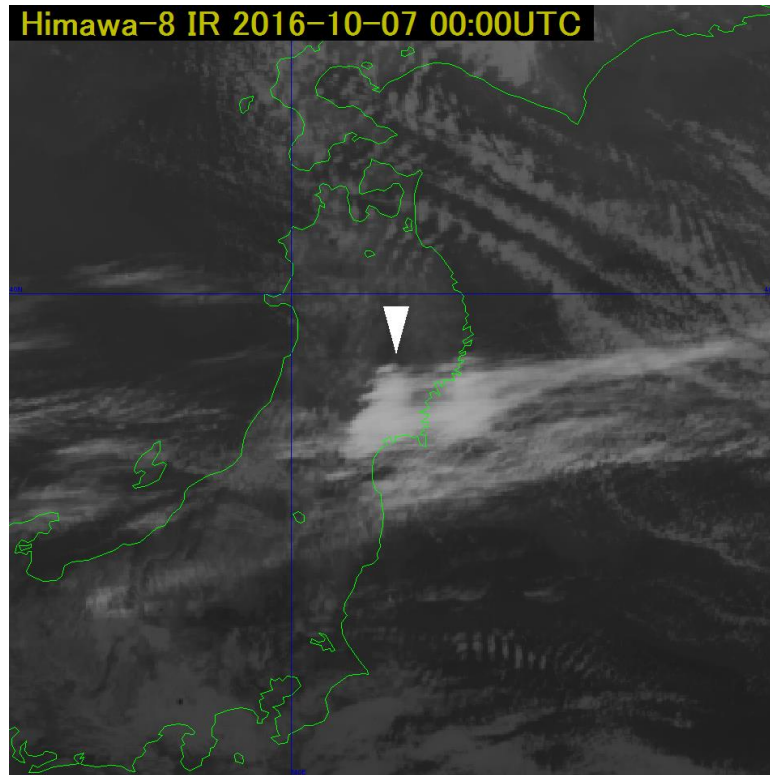


Fig. 3-3-2. B03 visible image for 00:00 UTC on 7 October 2016

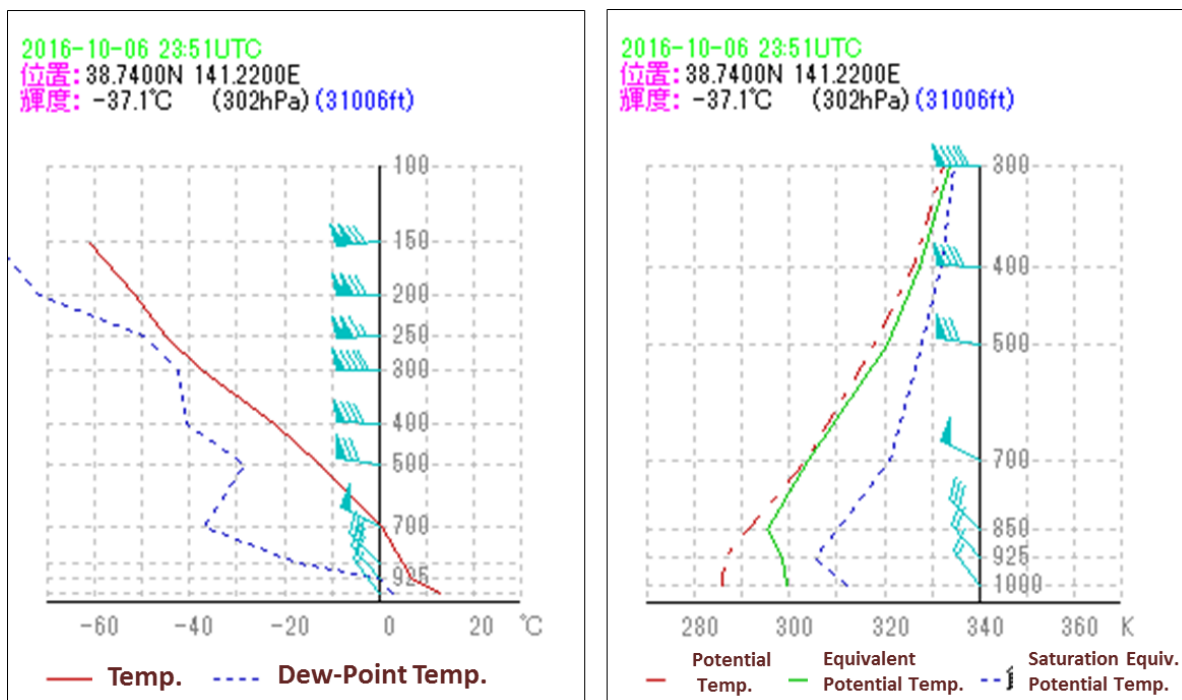


Fig. 3-3-3. Emagram (left) and potential temperature emagram (right) for 00:00 UTC on 7 October 2016

In Day Convective Storm RGB image, it should be noted that orographic Ci appears in the same color as active cumulonimbus areas accompanying strong updrafts (Fig. 3-3-4) with

stable stratification and strong winds over mountainous areas. Ice-crystal sizes in cirrus cloud are similar to those of the cloud top of active cumulonimbus accompanying strong updrafts.

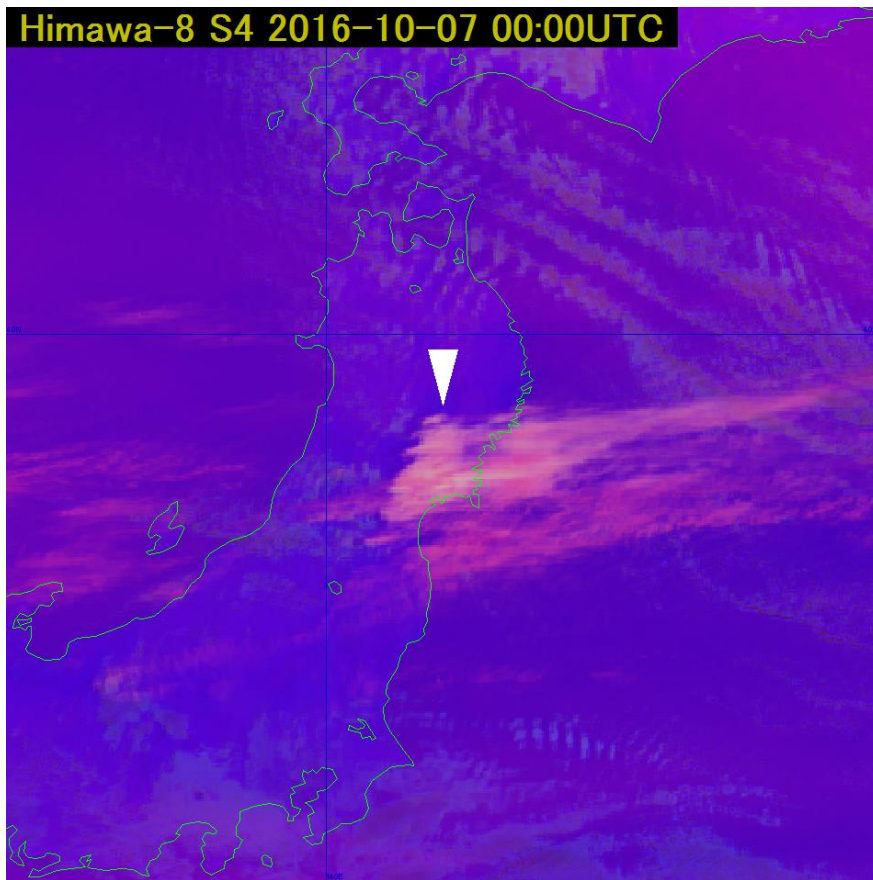


Fig. 3-3-4. Day Convective Storm RGB image for 00:00 UTC on 7 October 2016

3.4. Anvil Ci

Cumulonimbus (Cb) clouds in phases between the most active and the dissipation phases often take on an anvil-like structure due to horizontal Ci flow suppressed by the tropopause at the cloud top.

Anvil-type Ci extends in a feather-like manner mostly on the leeward side from cumulonimbus with a fuzzy edge (Fig. 3-4-1). The cloud top height of anvil Ci is roughly equivalent to the center of cumulonimbus, but the formation is not accompanied by strong rain. Hence, it is important to distinguish this cloud type from Cb centers.

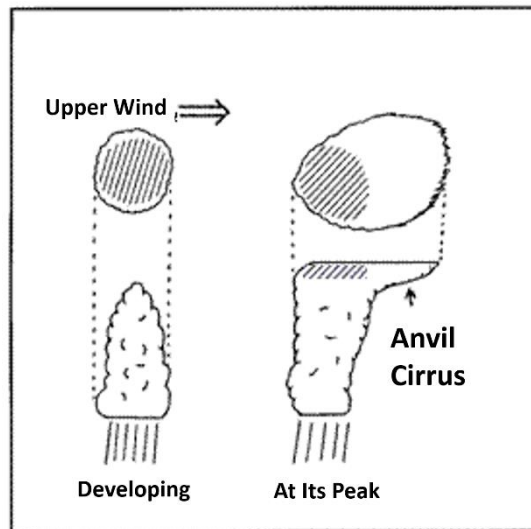


Fig. 3-4-1. Anvil Ci

Figures 3-4-2 and 3-4-3 show visible and infrared image of cumulonimbus over the Boso Peninsula in Japan's Chiba Prefecture with anvil Ci extending from the center for 05:00 UTC on 4 August 2016. The cumulonimbus center appears as an uneven part at the cloud surface in the visible image.

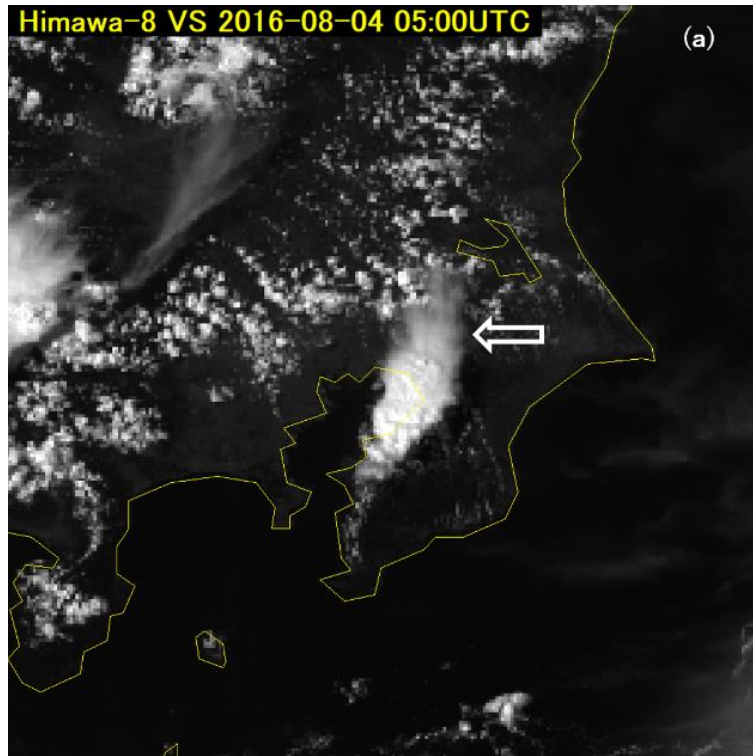


Fig. 3-4-2. B03 visible image for 05:00 UTC on 4 August 2016

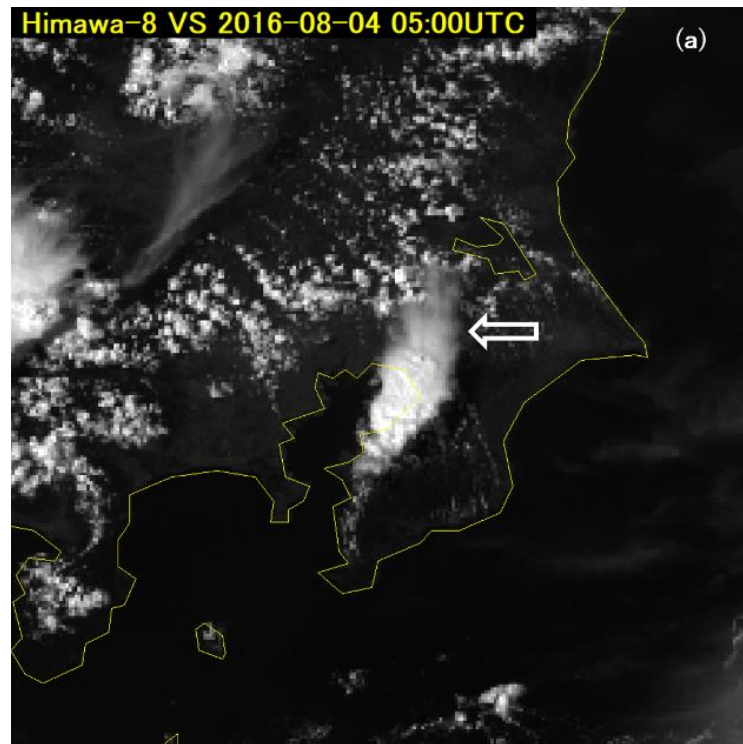


Fig. 3-4-3. B13 infrared image for 05:00 UTC on 4 August 2016

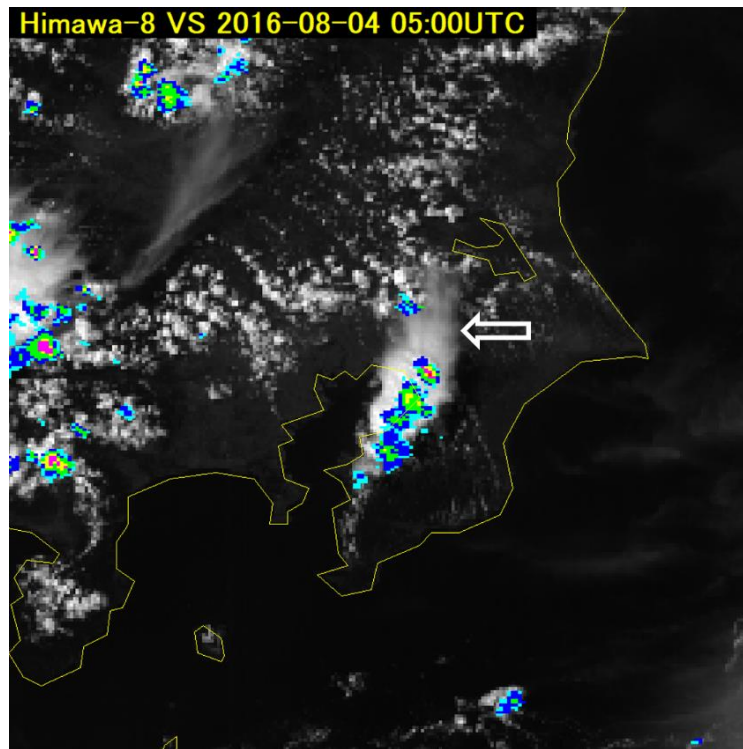


Fig. 3-4-4. B03 radar composite image for 05:00 UTC on 4 August 2016

Figure 3-4-4 shows an overlay of visible image and radar echo from the same time period. The cumulonimbus center is accompanied by precipitation observed as radar echoes. However, the anvil Ci extending northeastward from the center of the cumulonimbus was not visualized by radar because it was an upper-cloud type. Figure 3-4-5 shows shoreline cloud in Kanagawa Prefecture with anvil Ci on the left.



Fig. 3-4-5. Anvil Ci as per the cumulonimbus shown in Fig. 3-4-4

3.5. Bulge

Bulge is a phenomenon involving convex expansion with anticyclonic curvature of frontal cloud bands toward a cold polar side. It represents a developing cloud area with a warm wet wind current rising in correspondence with cyclonic development or a frontal wave brought by an approaching trough. The curvature increases as the cloud area develops, and expansion toward the cold side may also be seen in non-developing cloud areas. Temporary formations with no continuation are not classified as bulges. In Fig. 3-5-1, bulges are seen between Pyongyang and Lake Khanka (arrows).

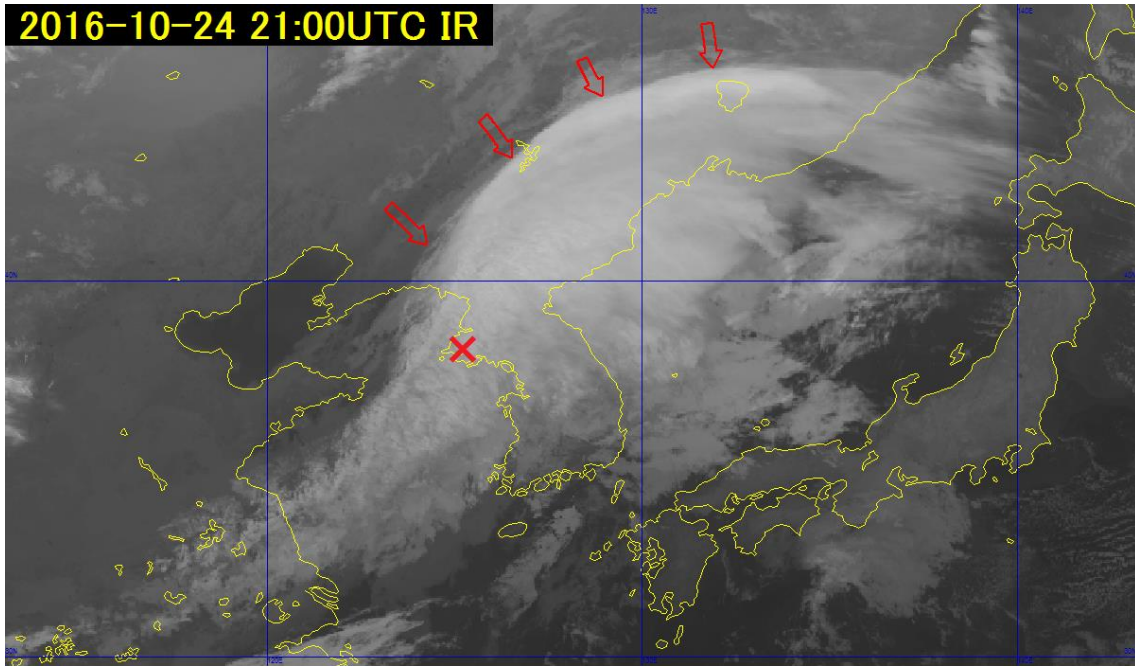


Fig. 3-5-1. B13 infrared image for 21:00 UTC on 24 October 2016

3.6. Hook Patterns

Anticyclonic curvature in developing cloud areas may increase at the northern edge and present cyclonic curvature at the southwestern edge in a formation known as a hook, representing the presence of cold air entering from the rear of the cloud area. There is also a rough correlation between hooks and ground-level low-pressure centers (Section 5.2.1). Internationally, comma-shaped forms observed by radar or otherwise are more broadly called hook patterns. Figure 3-5-1 shows a cloud area with a hook pattern by the Korean Peninsula (red cross).

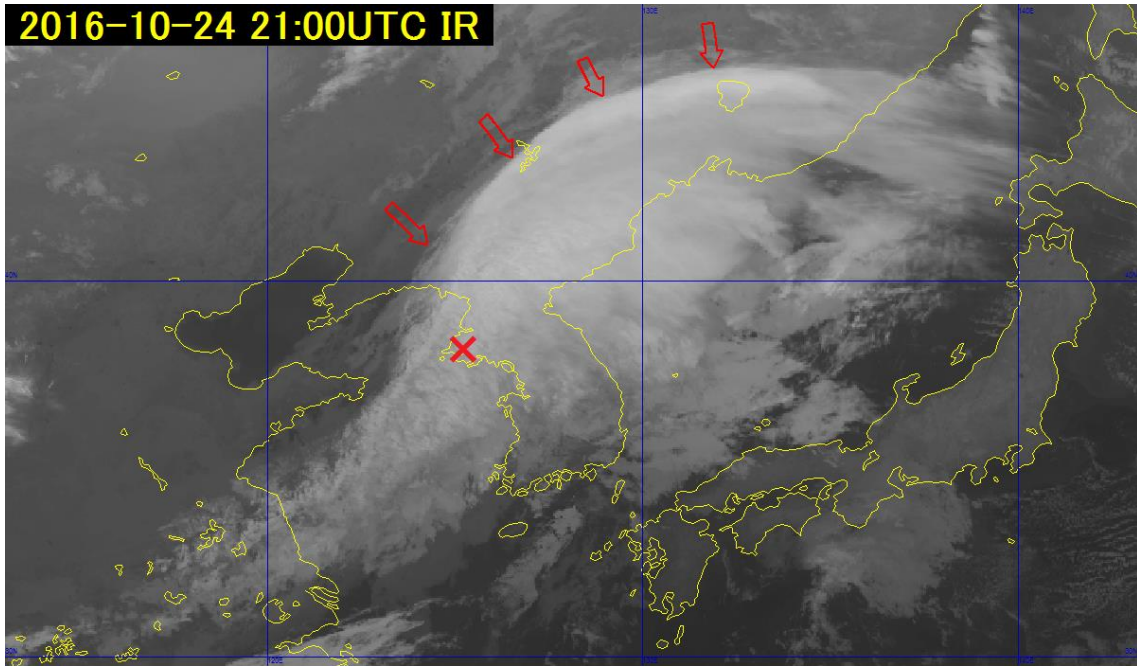


Fig. 3-5-1. B13 infrared image for 21:00 UTC on 24 October 2016

3.7. Lee Wave Clouds

Lee wave clouds align in a regular pattern leeward of mountain ranges and island forms. Figure 3-7-1 shows such cumulus and stratocumulus clouds aligning parallel to the Ou mountains. With long thin forms such as mountain ranges, these clouds have a strike parallel at the leeward side.

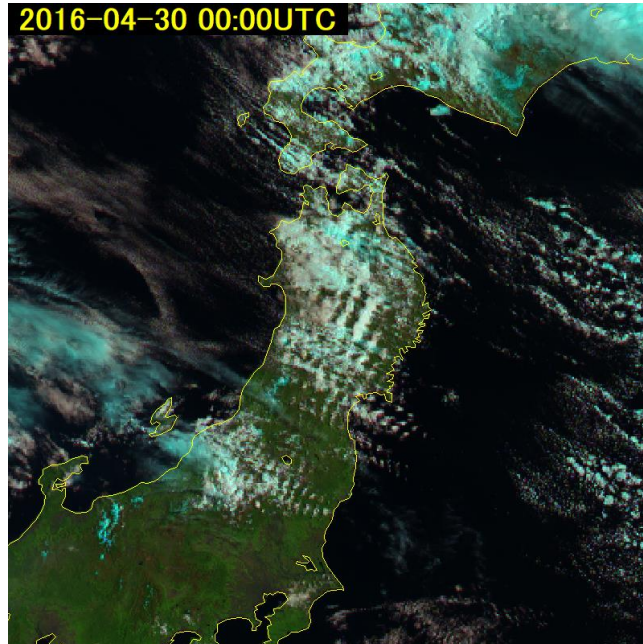


Fig. 3-7-1. Natural color RGB image for 00:00 UTC on 30 April 2016

3.7.1. Environmental Conditions for Lee Wave Clouds

The following conditions support lee wave cloud formation:

1. The wind direction is roughly steady through a thick layer up to the upper layer orthogonal to the strike of an obstacle.
2. Absolutely steady conditions exist throughout a very thick space up to the upper layer.
3. Sufficient water vapor for cloud formation is present.
4. Wind speed around the mountain top is above 10 m/s.
5. Stratospheric development with a decreasing Scorer number is observed.

Figure 3-7-2 shows a potential temperature emagram for Akita at the time of lee wave cloud emergence with the following characteristics:

1. The wind direction is roughly steady throughout the thick layer up to the upper layer west-northwest to northwest, approximately at a right angle to the strike of the Ou mountains.

Utilization of Meteorological Satellite Data in Cloud Analysis

2. Neutrality is observed up to around 700 hPa from the equivalent potential temperature, with convective stability above this region along with static stability.
3. Humidity exceeds 80% between 925 and 700 hPa, providing sufficient water vapor for lower clouds to form.
4. The Ou mountain altitude is 1,500 – 2,000 m, with a wind speed of 14 m/s at 850 hPa and 17 m/s at 800 hPa.
5. Wind speed increases from the lower to the upper layers, with the Scorer number decreasing toward the upper layer.

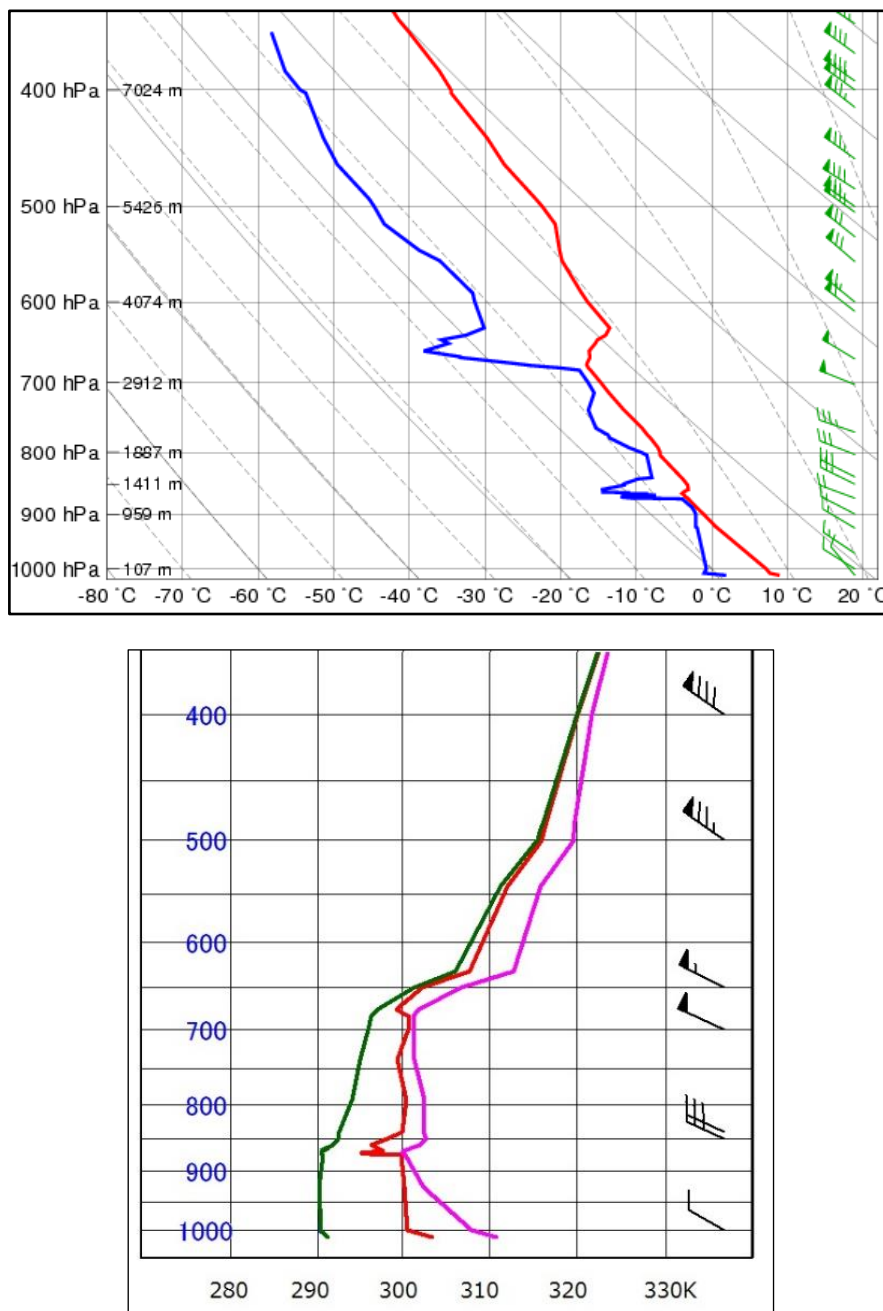


Fig. 3-7-2. Emagram (upper) and potential temperature emagram (bottom) for Akita at 00:00 UTC on 30 April 2016

Green: potential temperature; red: equivalent potential temperature; pink: saturation potential temperature

The lee wave theory proposes that intervals of such clouds are directly proportional to wind speed (Section 3.7.2). The potential for related turbulence along mountain lee waves must also be examined, with consideration of elements other than wind speed such as inversion layer altitude, vertical stability and mountaintop formations. Lee wave clouds observed in satellite imagery may not be directly associated with turbulence, but can be seen as an indicator of potential for the phenomenon. In addition, as such waves tend to move to the upper-stream side of mountains, lee wave clouds may also appear slightly toward the windward side rather than only on the leeward side (Fig. 3-7-3).

3.7.2. Relationship Between Intervals of Lee Wave Clouds and Wind Speed

Figure 3-7-4 shows infrared image and brightness temperatures for lee wave clouds with a top at around -10°C . Aerological observation in Akita revealed temperatures of -6.8°C at 800 hPa and -14.7°C at 700 hPa, suggesting a lee wave cloud altitude of around 2,500 m. Lee wave cloud intervals are proportional to wind speed, which allows wind speed estimation.

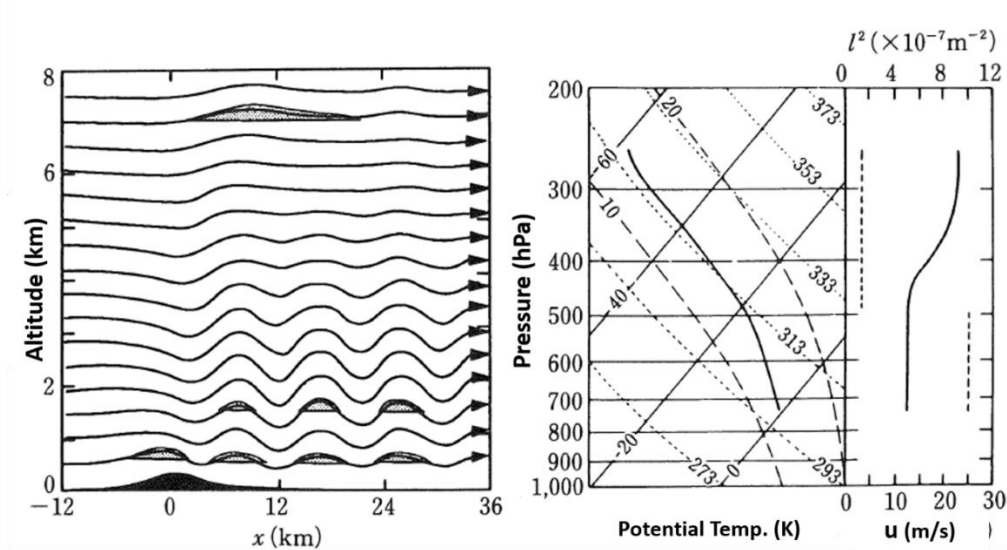


Fig. 3-7-3. Schematic diagram of lee wave clouds (Ogura, 1997)

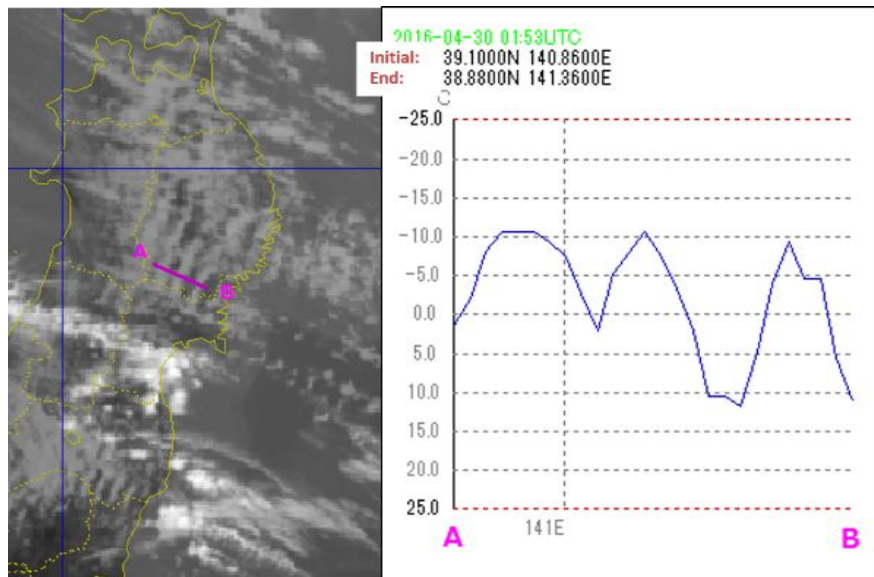


Fig. 3-7-4. B13 infrared image and brightness temperatures (line section indicated by the yellow arrow) for 02:00 UTC on 30 April 2016

Supplementary Information

With wind speed as U (in m/s) and the wavelength of leeward wind as λ (in km), the relationship can be written as follows (Corby G.A., 1957):

$$U = 1.7 \lambda + 4.8$$

Measuring λ in satellite imagery, $5 \text{ km} < \lambda < 10 \text{ km}$.

By substituting the values into the equation,

$$13.3 \text{ m/s} < U < 21.8 \text{ m/s} \text{ (where } \lambda = 8 \text{ and } U = 18.4)$$

Aerological observation in Akita shows 14 m/s at 850 hPa, 17 m/s at 800 hPa, and 26 m/s at 700 hPa. The height of lee wave clouds estimated from brightness temperatures is around 2,500 m, which is roughly in agreement with the equation value.

* Scorer number

This dimensionless quality is represented by the equation below.

h : mountain height; s : static stability;

g : gravitational acceleration;

u : wind speed; z : altitude

$$h^2 \left(\frac{sg}{u^2} - \frac{1}{u} \frac{\partial^2 u}{\partial z^2} \right)$$

3.8. Open Cells

In satellite imagery, cloud patterns forming a donut shape or a U-shape in otherwise cloudless areas are called open cells. Those consisting of convective clouds descend to previously cloudless areas (Fig. 3-8-1) with vertical circulation ascending within the wall cloud surroundings. Donut patterns are sustained with smaller vertical wind shear and lower wind speeds. Faster winds and larger vertical wind shear may cause the ring to collapse with no open cell pattern formation.

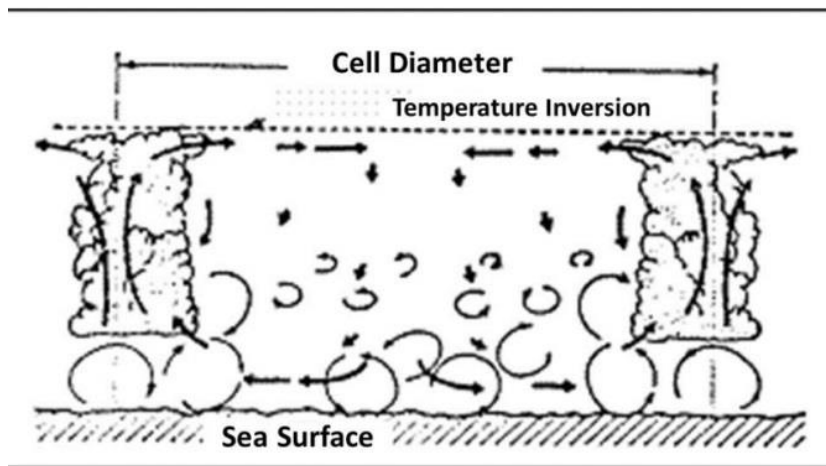


Fig. 3-8-1. Open cell formation (Asai, 1983)

Bader *et al.* (1995) described how the shape of open cells depends on lower-layer wind speed (Fig. 3-8-2). Such cells appear in polygon or donut form with winds below 20 kt in the lower layer, whereas the ring around cloudless areas begins collapsing at higher wind speeds to form a U-shape. As wind speed rises, formation irregularity increases with further spreading along the current.

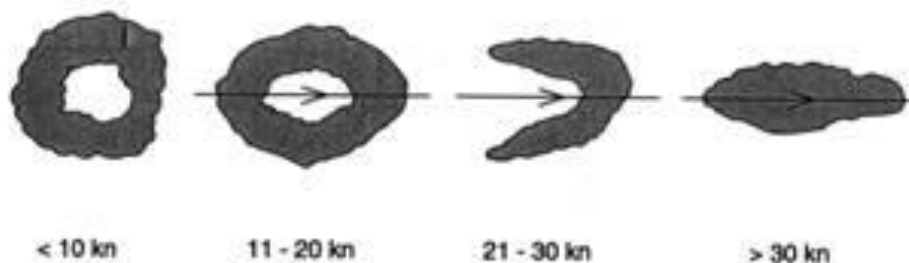


Fig. 3-8-2. Open-cell development with specific wind speeds (in knots)
Arrows indicate wind direction (Bader *et al.* 1995)

As open cells are associated with large temperature differences between cold air and warm seas surfaces, they can be used to estimate the strength of cold air running from the rear of

developed cyclones. Such patterns tend to emerge in lower layers when strong cyclonic currents are present. Cold advection is generally stronger with larger temperature differences between air and the sea surface.

Figure 3-8-3 shows True-Color Reproduction image for visible bands from 00:00 UTC on 12 February 2016, with various cloud patterns emerging in a cold area over sea areas east of Japan. The pattern marked O is an open cell in cyclonic circulation. Figure 3-11-2 (Section 3.11) shows the corresponding surface weather chart.

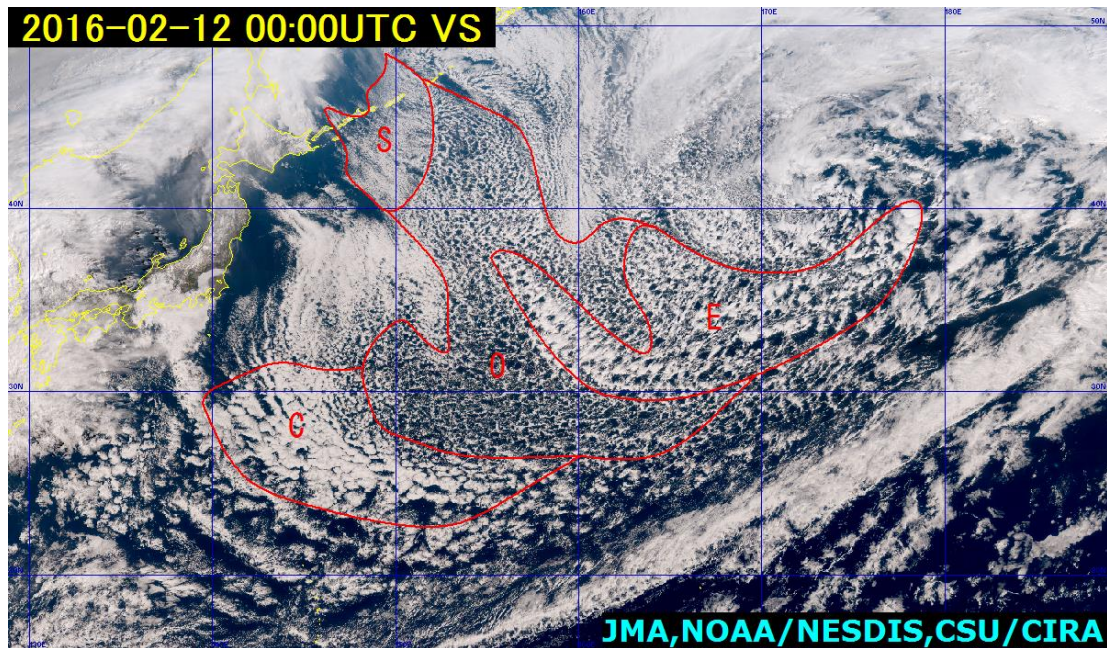


Fig. 3-8-3. True Color Reproduction image for 00:00 UTC on 12 February 2016

3.9. Closed Cells

In satellite imagery, polygonal and dense clouds forming a cell surrounded by a clear area are called closed cells. These are stratocumulus clouds with relatively small vertical wind shear and wind speeds often under 20 Kt. With a cloud top restrained by an inversion layer, they tend to emerge in areas of anticyclonic currents in the lower layer corresponding to the southeastern quadrant. As shown in Fig. 3-9-1, the central cloud is formed by an updraft with vertical circulation descending in the surrounding clear area.

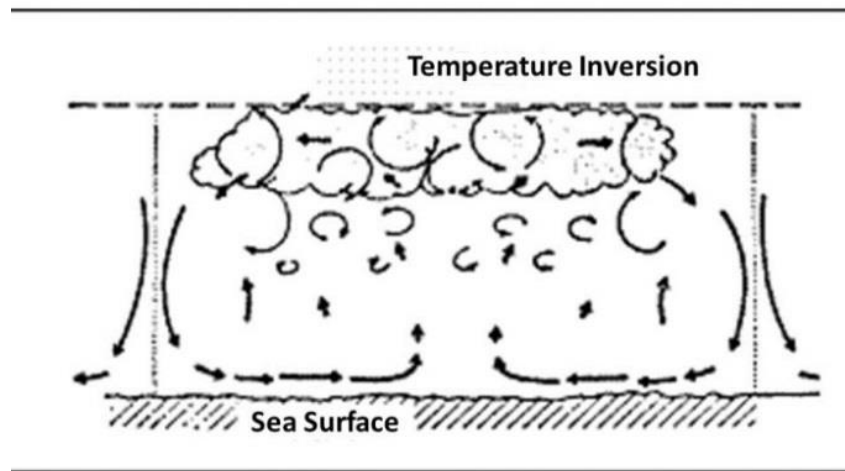


Fig. 3-9-1. Closed cell model (Asai, 1983)

Closed cells emerge with smaller temperature differences between air and the sea surface than open cells, and may form with less cold air entering or by weakened cold areas that turn open cells into closed cells. The open/closed status is generally based on the strength of the cold. The border between a region with an open cell and one with a closed cell may indicate jet stream positioning in the lower layer, as shown in Fig. 3-9-2 (Bader *et al.*, 1995).

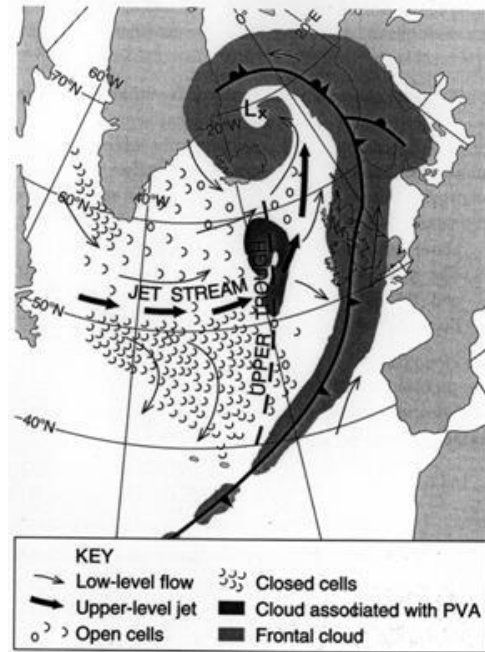


Fig. 3-9-2. A general cell-form cloud pattern in a cold area and a synoptic field (Bader *et al.*, 1995)

Cloud pattern C in Fig. 3-8-3 (Section 3.8) is a closed cell in circulation at the southeastern quadrant of an anticyclone, presumably corresponding to an area with weakened cold.

3.10. Cloud Streets

In satellite imagery, parallel patterns of Cu and Cg clouds are called cloud streets, with near-parallel tracks to lower-layer winds and a roughly uniform cloud top height. Vertical shear in the wind direction is relatively small inside the cloud layer but larger than that of open/closed cells, creating a roll formation (with lines or bands) parallel to the shear of lower wind. As seen in Fig. 3-10-1, there is helical motion of the air parcel in the roll-shaped convection and formation of convective cloud in the upper part of the updraft region.

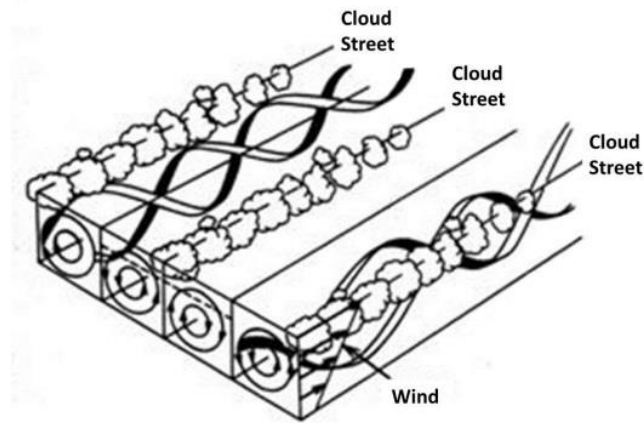


Fig. 3-10-1. Roll-shaped convection (Asai 1996)

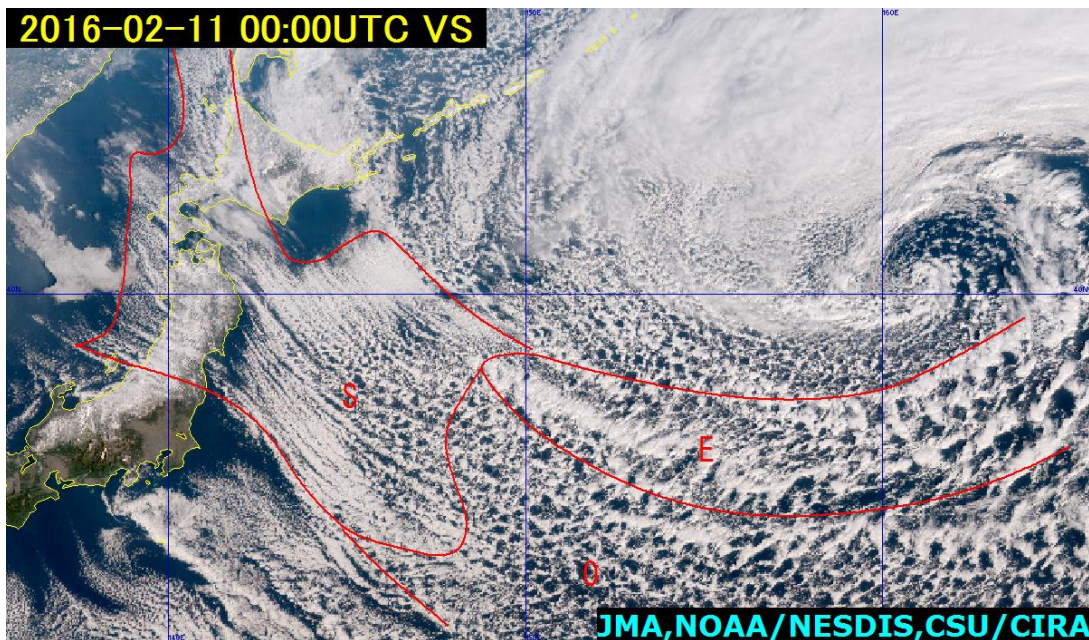


Fig. 3-10-2. True Color Reproduction image for 00:00 UTC on 11 February 2016

3.11. Enhanced Cu

Satellite imagery of open cell regions consisting of Cu in cold areas behind cyclones shows Cb and Cg clouds in areas referred to as enhanced Cu. These arise due to intense cold air migrating southward from behind a developed cyclone, activating Cu into Cb or Cg. The presence and intensity of cold air can be estimated from the characteristics of the enhanced Cu.

Figure 3-11-1 shows a day snow-fog RGB composite image of day snow-fog on the same day as Fig. 3-8-3 (Section 3.8), indicating the cloud pattern E as enhanced Cu. Orange indicates thick cloud areas with precipitation, which are more active with a higher cloud top than other parts of the open cell, and more organized with anvil cloud. Figure 3-11-3 shows a 500 hPa upper-level weather chart for 00:00 UTC on 12 February 2016. A trough accompanying cold air below -36°C is seen moving eastward, causing Cu to develop into Cb or Cg due to convective instability.

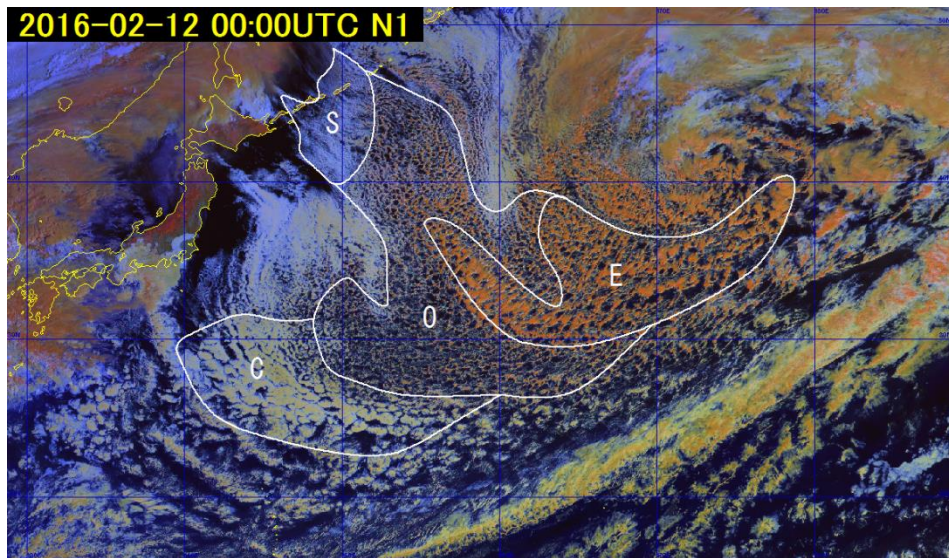
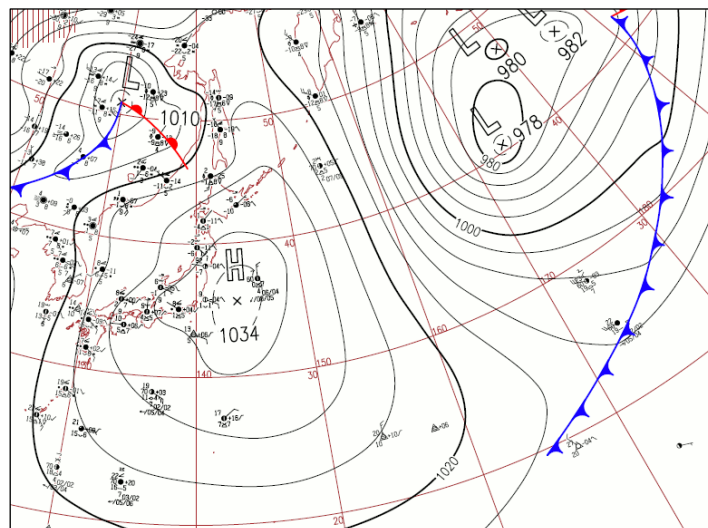


Fig. 3-11-1. Day snow-fog RGB composite image for 00:00 UTC on 12 February 2016



Chapter 3. Cloud Patterns

Fig. 3-11-2. Surface weather chart for 00:00 UTC on 12 February 2016

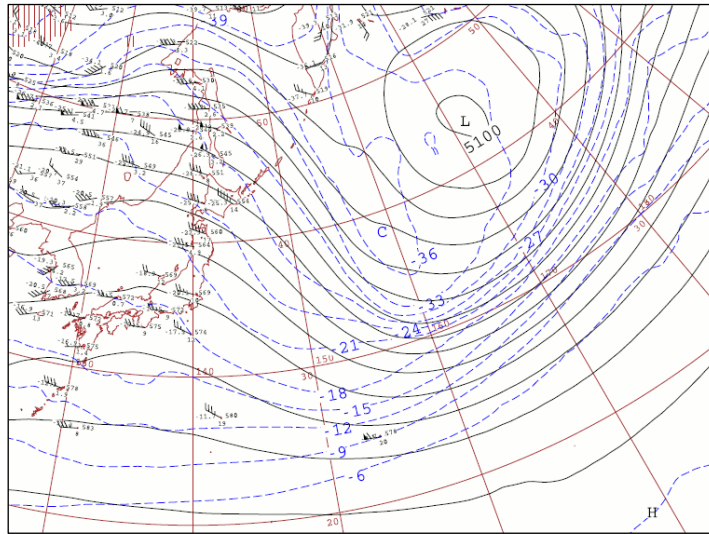


Fig. 3-11-3. 500 hPa upper-level weather chart for 00:00 UTC on 12 February 2016

3.12. Cb Cloud Clusters

Cb is often observed as individual clouds, but may also aggregate to form large parcels called cloud clusters or Cb clusters. Clusters are composed of convective clouds of various sizes at different stages during development, reaching up to several hundred kilometers on a horizontal scale. Meso-convective systems such as squall lines and multi-cells are recognizable in radar imagery, and cloud clusters (convective systems on a larger scale) are recognizable in satellite imagery, often appearing in the tropics or over continental areas in summer.

In the field of satellite observation, Maddox (1980) defined α -scale mesoscale convective complexes (MCCs) as systems producing extreme phenomena such as tornadoes, hail and thunderstorms over north America. MCCs are defined as cloud areas with a top temperature below -32°C and a size exceeding 0.1 million km^2 (diameter: approx.: 350 km), with a near-circular formation (i.e., a major/minor axis ratio above 0.7) persisting for six hours or more. These tend to develop over continental areas between late evening and nighttime in unstable atmospheric conditions with weak forced convection on a synoptic scale. Figures 3-12-1 and 3-12-2 show MCC conditions observed by Himawari-8, with a near-circular cluster over 300 km in diameter (cloud area C) above China.

For the area around Japan, Iwasaki and Takeda (1993) investigated regional appearance characteristics of mesoscale cloud clusters during Asia's rainy season. Such clusters were defined as cloud areas with a brightness temperature below -50°C forming a circular or oval shape with a diameter over 100 km, a rim (particularly on the western side) exhibiting a large gradient of brightness temperature, and emergence in mid-latitudes. Clusters over Japan were found to generally have an average life span of less than 14 hours and an average maximum diameter of 170 km. Those with a larger maximum diameter tended to have a longer life span. Larger clusters with a maximum diameter over 200 km often emerged over continental areas, whereas smaller ones were more likely to emerge over sea areas. Around Japan, the majority of large cloud clusters emerged and developed over the East China Sea, with some bringing heavy rainfall to the Kyushu region.

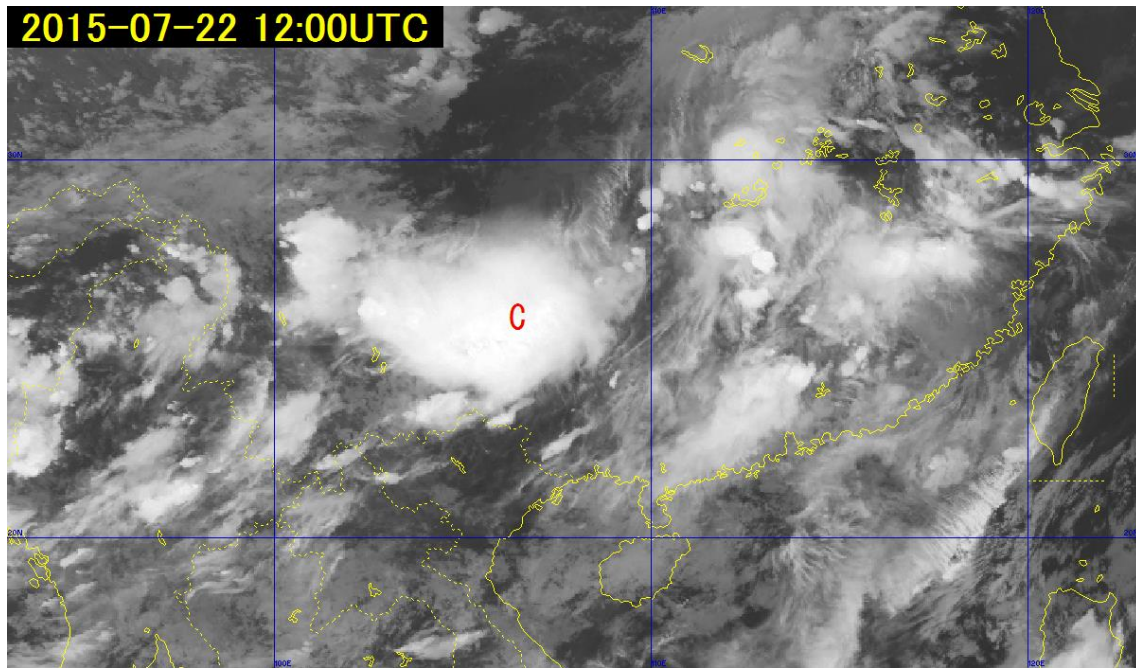


Fig. 3-12-1. B13 infrared image for 12:00 UTC on 22 July 2015

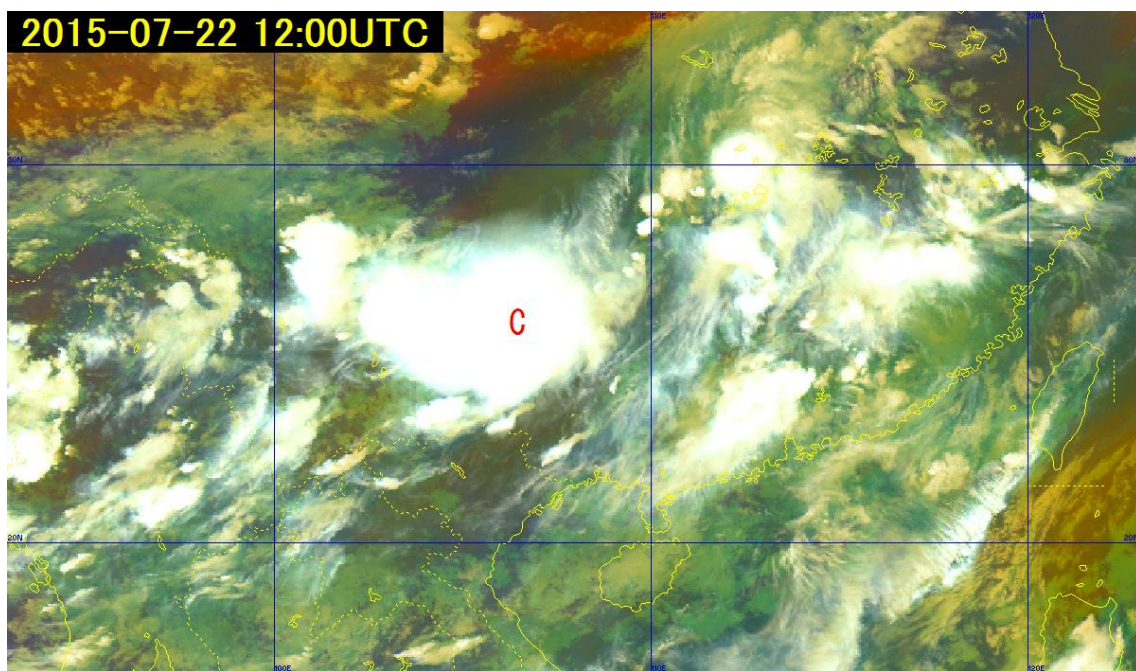


Fig. 3-12-2. Airmass RGB composite image for 12:00 UTC on 22 July 2015

Figures 3-12-3 and 3-12-4 show mesoscale cloud cluster conditions with a near-circular form over the western coast of Kyushu. Although on a smaller scale, the cluster is approximately equivalent to MCC conditions. It subsequently progressed eastward and weakened after passing over central Kyushu, causing heavy rainfall (hourly totals: 124.5 over Mt. Unzen in Nagasaki Prefecture, 150.0 mm in Kosa in Kumamoto Prefecture, 126.5 mm in Yamato in Kumamoto Prefecture). Figure 3-12-5 shows a surface weather chart for the period.

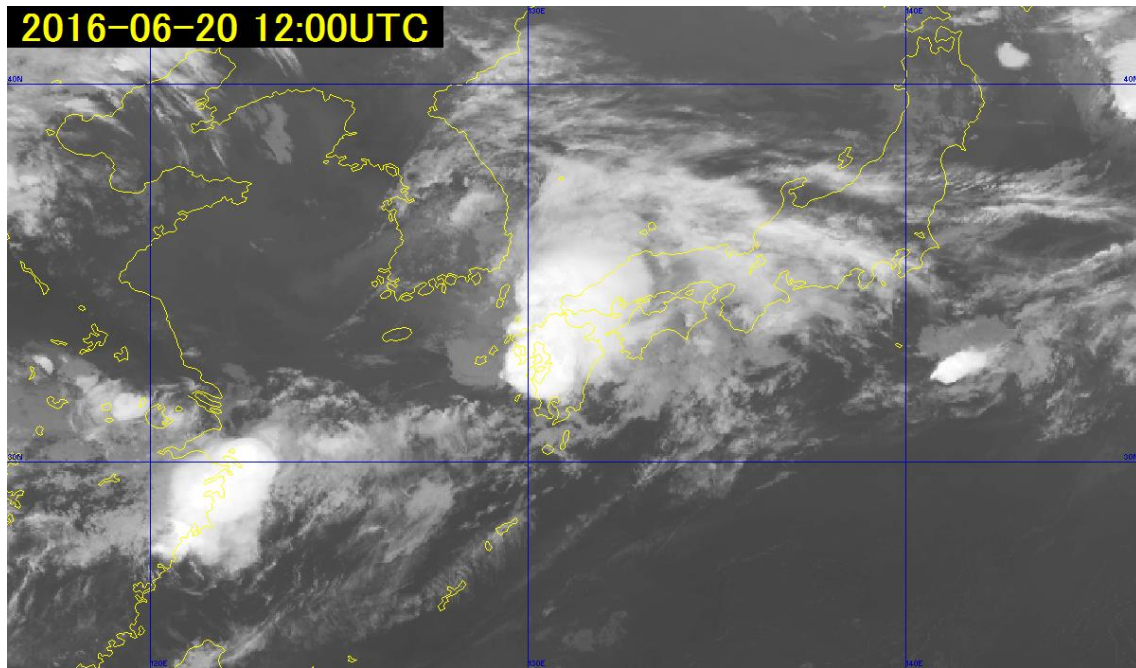


Fig. 3-12-3. B13 infrared image for 12:00 UTC on 20 June 2016

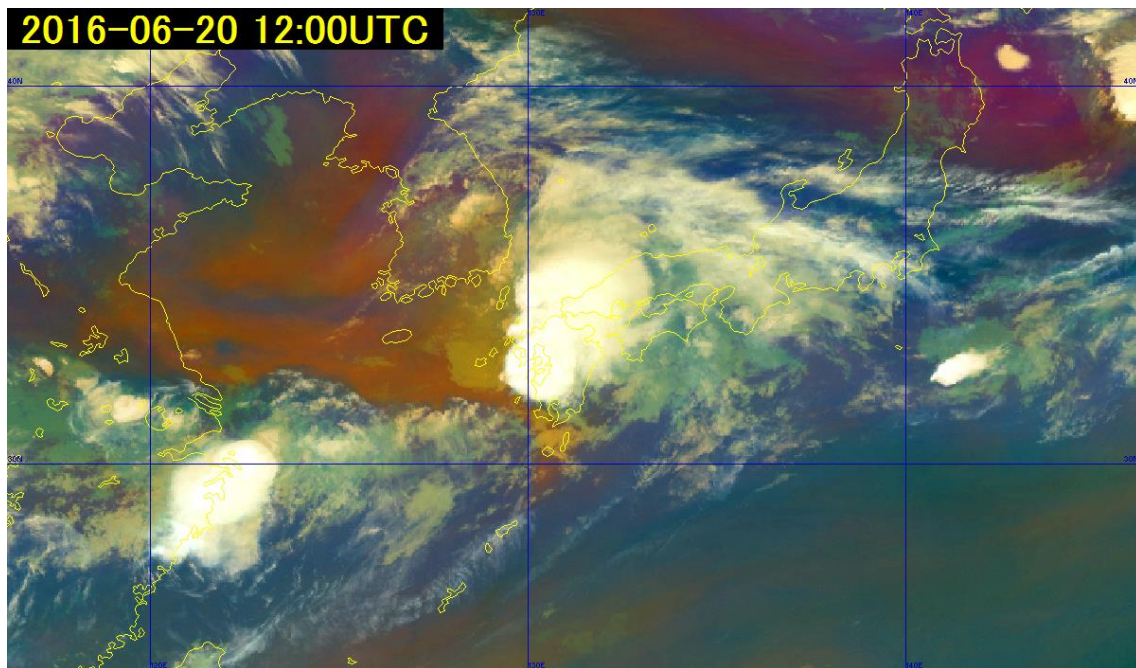


Fig. 3-12-4. Airmass RGB composite image for 12:00 TC on 20 June 2016

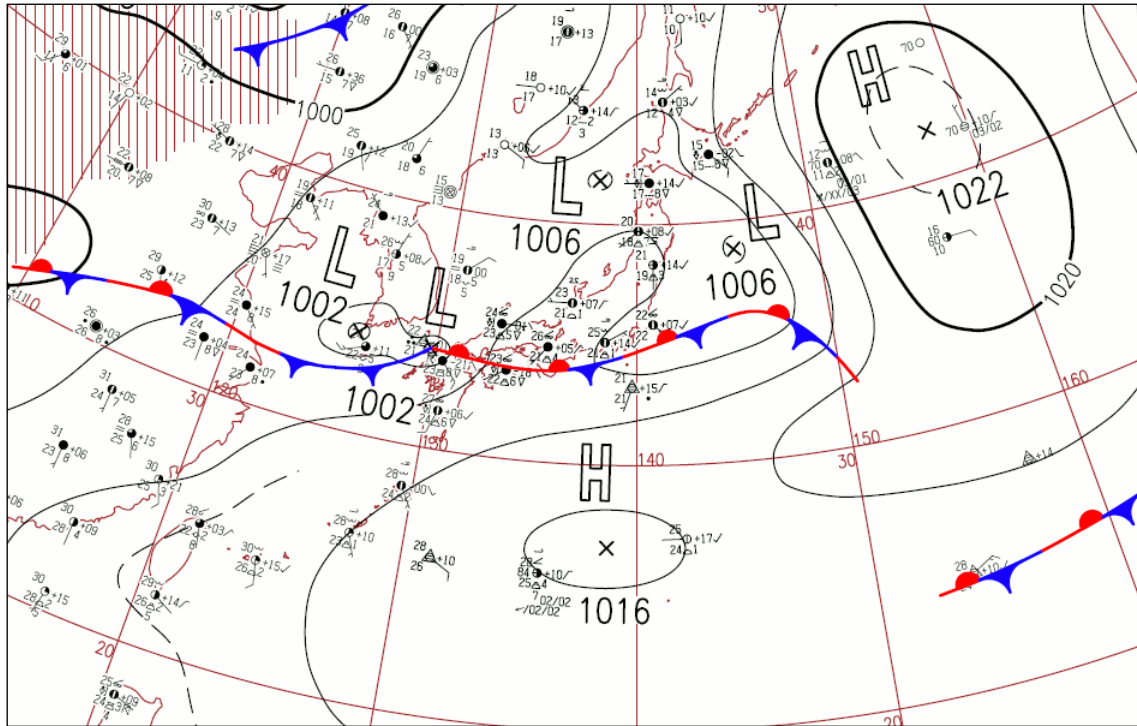


Fig. 3-12-5. Surface weather chart (prompt report) for 12:00 UTC on 20 June 2016

3.13. Central Dense Overcast (CDO) areas

CDOs are circular cloud areas with a smooth cloud top formed by an assemblage of Cb around the eye and center of typhoons. These form when a typhoon is developing, and act as an indicator of typhoon intensity in satellite observation. Figures 3-13-1, 3-13-2 and 3-13-3 show image for typhoon Nepartak (T1601) in 2016, with red arrows surrounding the CDO cloud area.

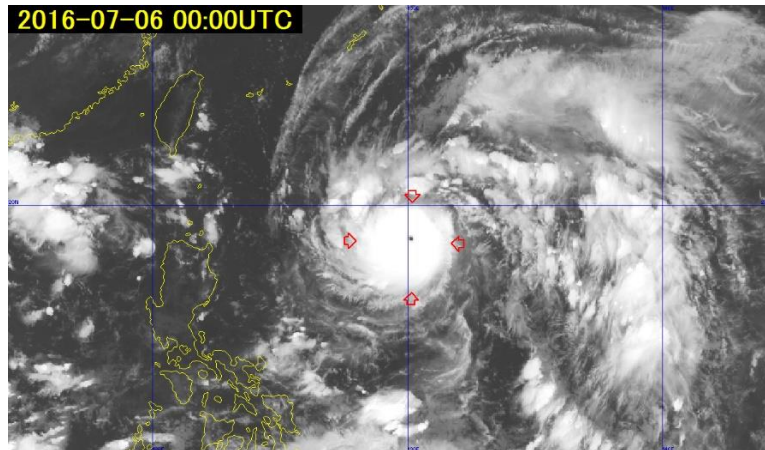


Fig. 3-13-1. B13 infrared image for 00:00 UTC on 6 July 2016

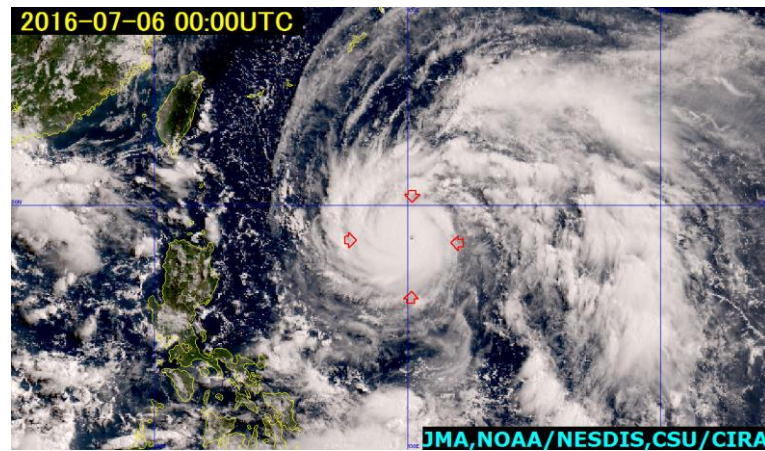


Fig. 3-13-2. True Color Reproduction image for 00:00 UTC on 6 July 2016

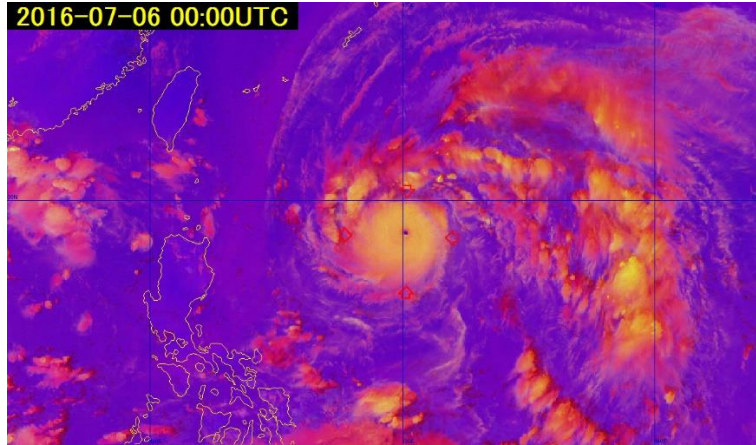


Fig. 3-13-3. Day convective storm RGB composite image for 00:00 UTC on 6 July 2016

3.14. Carrot-Shaped Clouds

These clouds are shaped like a carrot or the tip of a calligraphy brush, with gradual thinning toward the middle and upper layers windward. They consist of Cb cloud streets spreading from the windward to the leeward side and anvil Ci brought by upper winds. They are often associated with heavy rain, gusting winds, storm conditions and hail, particularly at the tip. Monitoring of their emergence and migration routes is essential.

MSC (1991) reported that convective masses containing individual Cb forms comprising carrot-shaped clouds tend to migrate downstream of middle and upper winds, occasionally stagnating, and sometimes occurring along convective cloud streets stretching windward. They usually have a life span of 10 hours and are associated with the following conditions:

1. Location predominantly over sea areas in connection with a ground-level low pressure center near fronts in warm areas
2. Prominence of warm moisture advection into the lower troposphere with dry air convection above
3. A relatively strong wind band, clear vertical shear and upper divergence in the upper troposphere

Figure 3-14-1 shows a carrot-shaped cloud southeast of Ishigaki Island in the region encircled in red, along with anvil Ci extending northeastward. In B03 visible image (Fig. 3-14-2), a Cb line stretches from the tip of the southern part toward the north-northeast. In the radar observation image shown in the upper-right panel of Fig. 3-14-1, echoes are observed with a precipitation intensity of 32 – 64 mm/h corresponding to the Cb street.

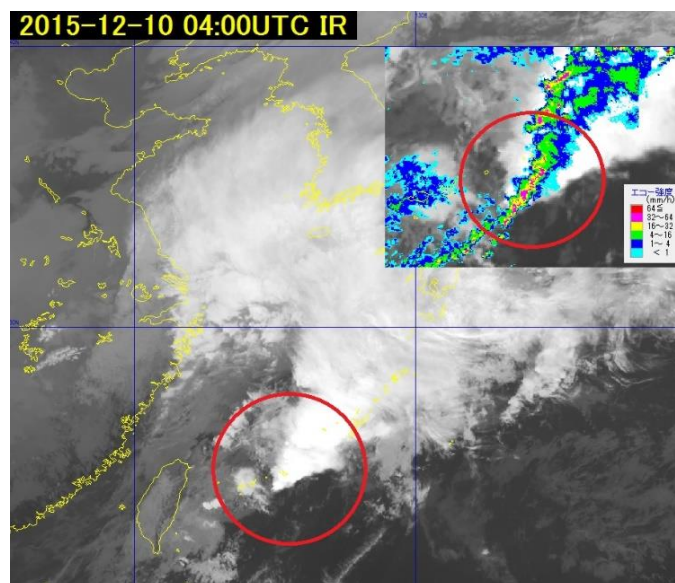


Fig. 3-14-1. B13 infrared image and radar precipitation intensity for 04:00 UTC on 10 December 2015

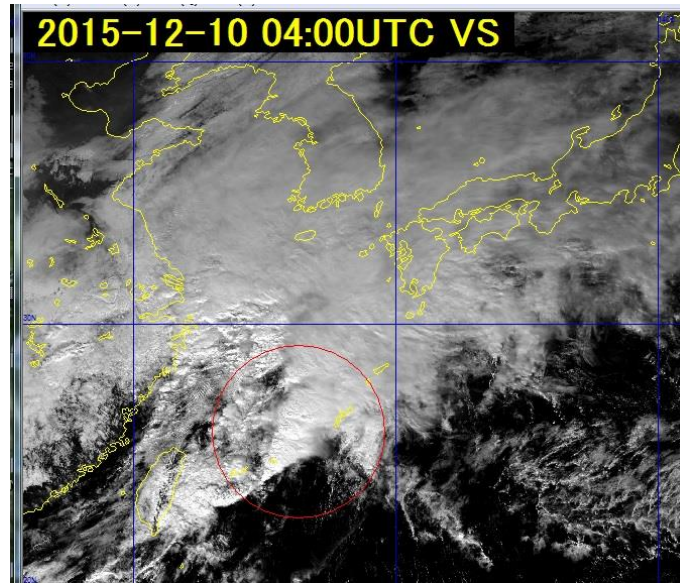


Fig. 3-13-2. B03 visible image for 04:00 UTC on 10 December 2015

Figure 3-14-3 shows an overlay of a B08 water vapor image and a wind diagram at 200 hPa altitude. It illustrates an accelerating zone (i.e. a divergent area) with faster wind speeds from the windward to the leeward areas of a carrot-shaped cloud. A strong wind band exceeding 100 kt is also seen to the north of the isotach. In the water vapor image, the carrot-shaped cloud emerges at the border of a relatively humid area and a dry area, indicating dry-air entry via the wind field.

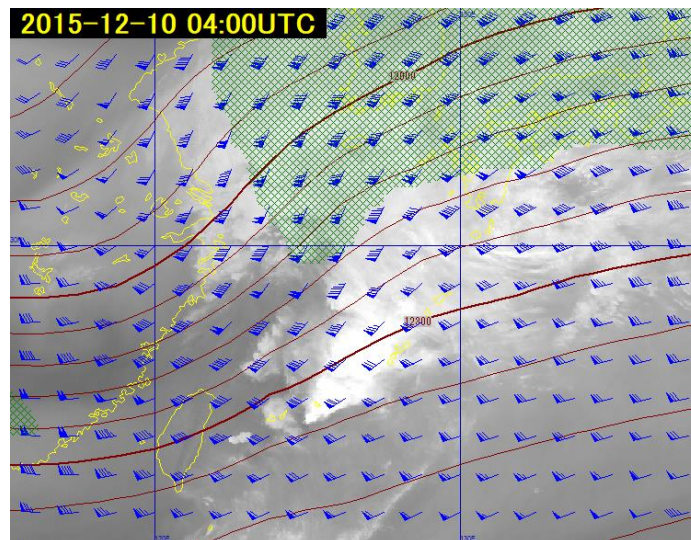


Fig. 3-14-3. B08 water vapor image for 04:00 UTC on 10 December 2015
200 hPa geopotential height (brown), winds, isotach (black)

Figure 3-14-4 shows wind and equivalent potential temperature at 850 hPa. In the area of the carrot-shaped cloud, a high equivalent potential temperature zone over 330 K enters from

the south into the warm area near the cold front. As in the cross-sectional view of Fig. 3-14-4, shear with high wind speeds toward the upper atmosphere is seen, corresponding to conditions increasing the likelihood of occurrence as described previously.

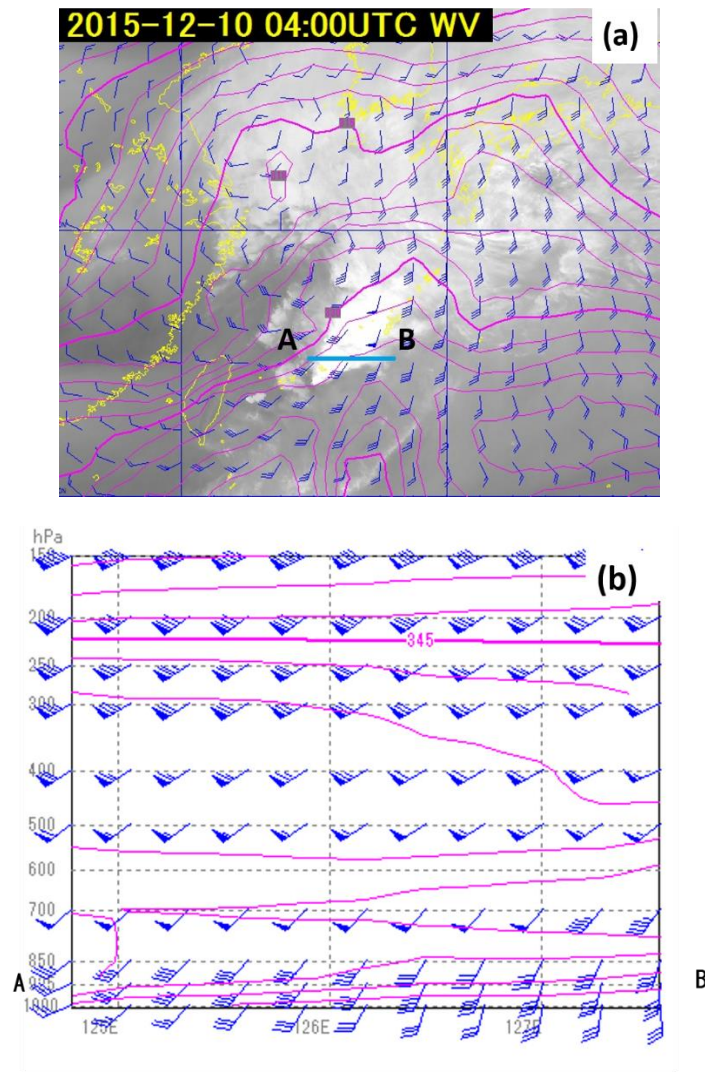


Fig. 3-14-4. B13 infrared image for 04:00 UTC on 10 December 2015 (a), with equivalent potential temperature at 850 hPa and winds (b). The lower panel shows a cross-sectional view along the blue line of the upper figure.

3.15. Cloud Bands

Cloud bands are areas in belt form with upper, middle and lower layers, or middle and lower layers accompanied by a front line (i.e., a frontal cloud band) or belt-form areas of convective clouds.

Figures 3-15-1 and 3-15-2 show a frontal cloud band (A-A) comprising middle and lower layers with 200 – 300 km widths between Japan's Kanto district and the northern area of the Sakishima islands for latitudinal lengths of around 2,000 km. Another band (B-B) comprising mostly convective clouds is also observed between the Kanto district and the southern area of mainland Okinawa.

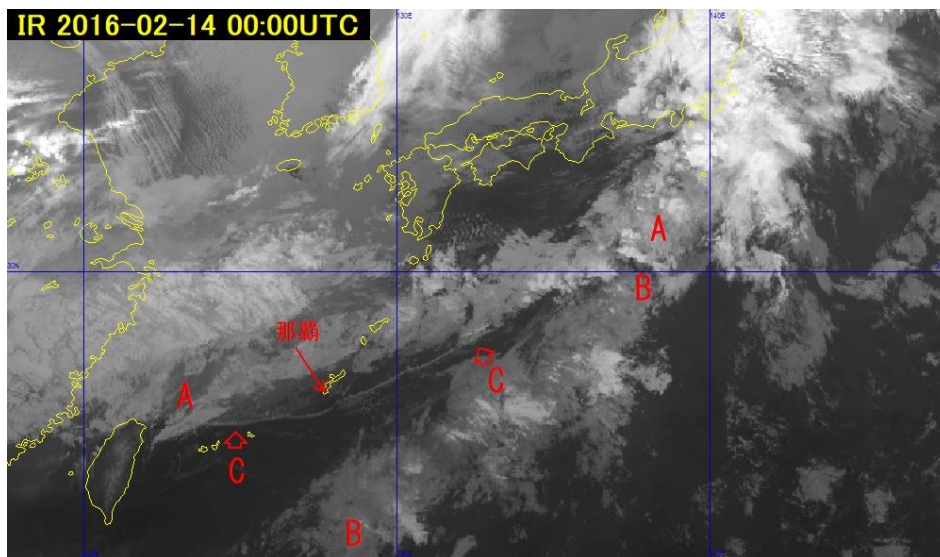


Fig. 3-15-1. B13 infrared image for 00:00 UTC on 14 February 2016

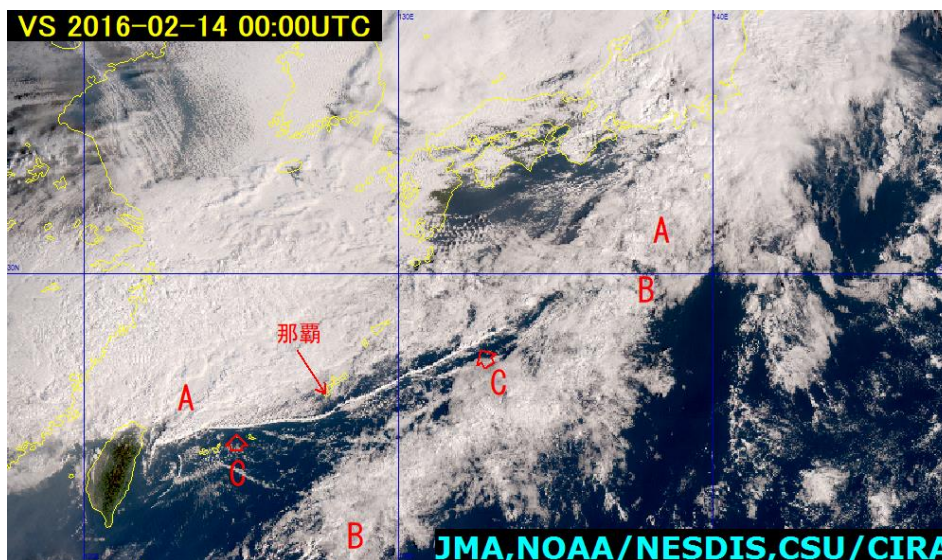


Fig. 3-15-2. True Color Reproduction image for 00:00 UTC on 14 February 2016

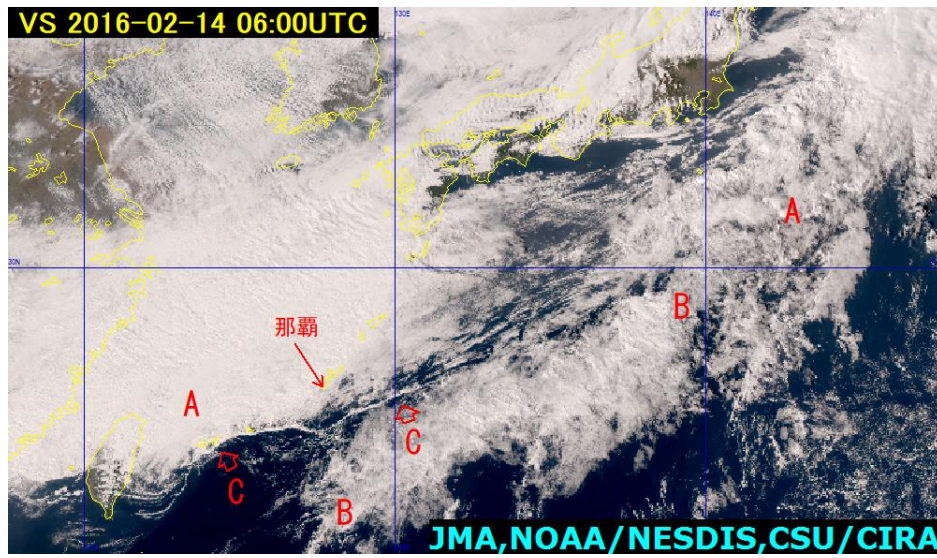


Fig. 3-15-3. True Color Reproduction image for 06:00 UTC on 14 February 2016

3.16. Cloud Lines

Cloud lines are strings of aligned convective clouds, with those containing Cb and Cg called Cb-Cg lines and those consisting solely of Cu called Cu lines.

In Figs. 3-15-1 and 3-15-2, the cloud line **A-A** stretches between the southern edge of Taiwan and the area offshore of Shikoku, while **C** and **D** stretch from west-southwest to east-northeast. **C** is a Cu line between the Sakishima Islands and the area offshore of Shikoku with convective clouds, and **D** around Taiwan contains Cg (i.e., a Cg-Cu line).

3.17. Rope Clouds

Rope clouds are long thin Cu formations with a usual width of around 10 – 30 km and in some cases lengths of 2,000 – 3,000 km. They are seen mainly over sea areas along the warm side of frontal cloud bands, often corresponding to cold fronts, as winds and temperatures vary beyond the cloud line. They often occur when frontal activity is weakened and the cloud line contains no developed convective clouds such as Cb or Cg.

The surface weather chart in Fig. 3-17-1 shows a cold front stretching over to the sea south of Okinawa from a cyclone with a center above the northern Sea of Japan, generating waves on the front seen around Awaji Island. This cold front corresponds to the cloud line **B**, presenting an example of an active convective cloud line corresponding to a cold front generating rope cloud that passed over mainland Okinawa at around 21:00 UTC on 13 February. In time-series AMeDAS for Naha (Fig. 3-17-2), rapid changes in wind direction and temperature decreases were observed with the passing of the rope cloud. The cloud line **C** was attenuated whilst descending south along with weakening of the cloud band **A-A** (Fig. 3-15-3).

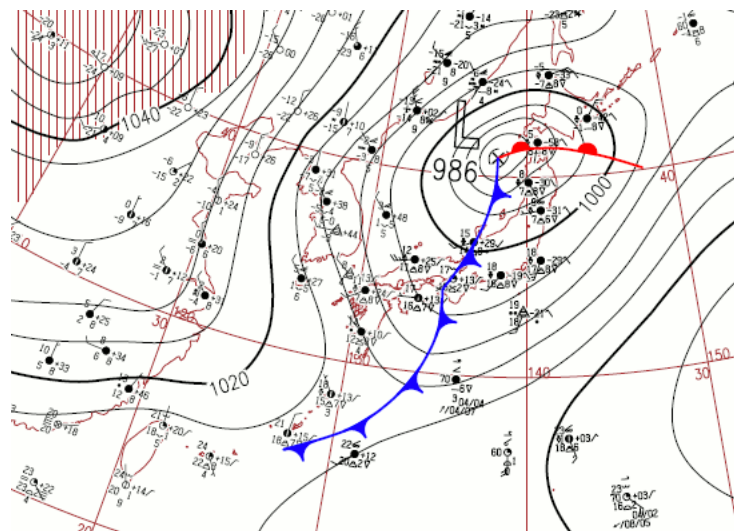


Fig. 3-17-1. Surface weather chart for 00:00 UTC on 14 February 2016

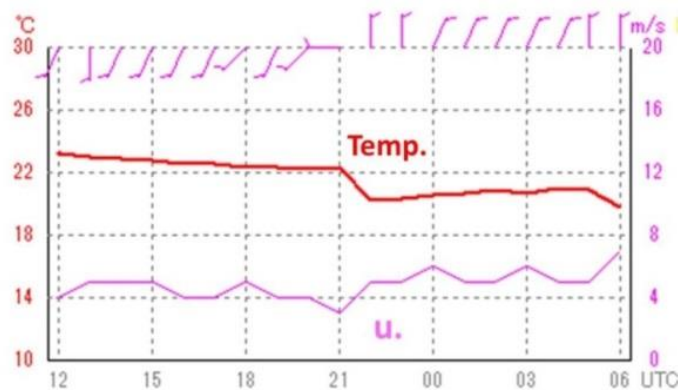


Fig. 3-17-2. Time-series AMeDAS data for Naha between 12:00 UTC on 13 February and

Chapter 3. Cloud Patterns

06:00 UTC on 14 February 2016, with temperatures in red and wind speeds in pink

3.18. Karman Vortices

As per the surface weather chart shown in Fig. 3-18-1, when winter pressure patterns collapse, anticyclonic conditions over continental areas move toward Japan. As northwestern winds weaken, vortices forming in relation to lower clouds leeward of the Jeju or Yakushima islands may subsequently align, rotating downstream anti-clockwise on the right and clockwise on the left (Fig. 3-18-2) in a phenomenon known as a Karman vortex.

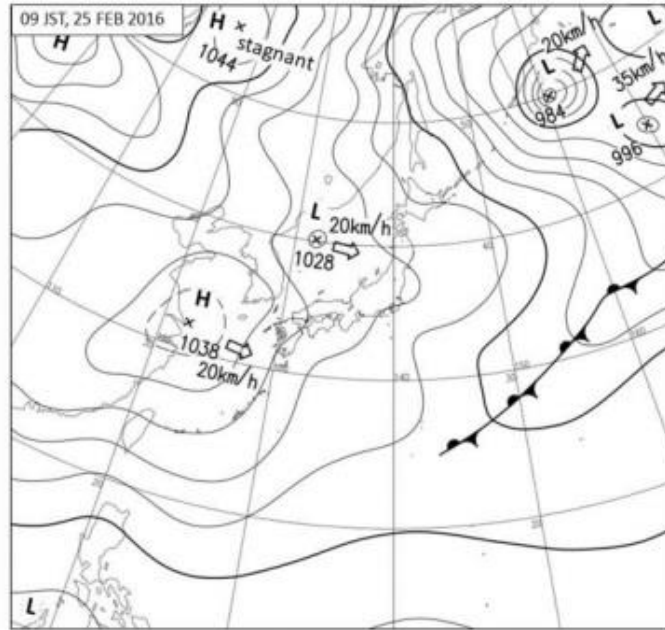


Fig. 3-18-1. Surface weather chart for 09:00 JST on 25 February 2016

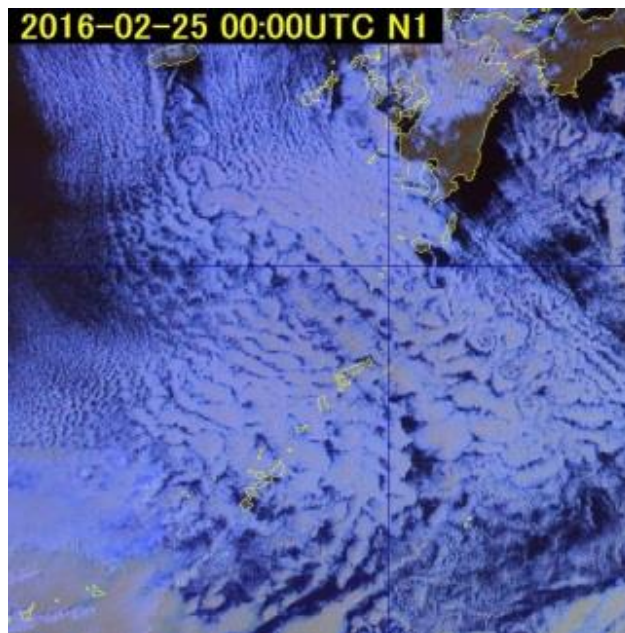


Fig. 3-18-2. Day Snow-Fog RGB composite image for 00:00 UTC on 25 February 2016

Karman vortices in satellite imagery are seen mainly as Sc leeward of island areas,

aligning periodically. Satellite imagery analysis by Hubert and Krueger (1962) and Thompson, Grower and Bowker (1977) proposed three conditions for Karman vortex occurrence:

1. Open sea covered by St or Sc under a strong temperature inversion layer
2. Persistent strong wind with a steady direction in the lower layer
3. Island topography with a mountain top exceeding hundreds of meters over the temperature inversion layer

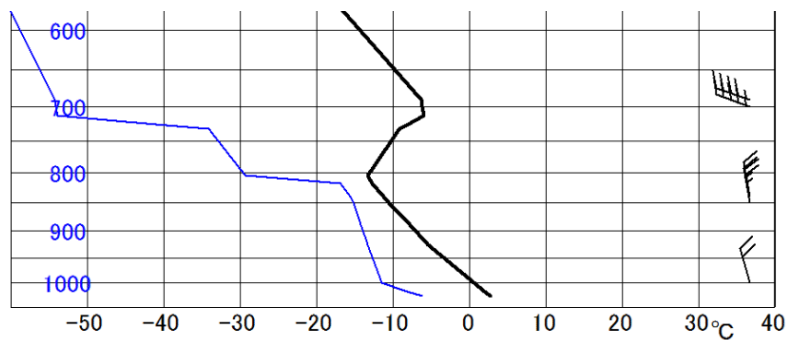


Fig. 3-18-3. Vertical profile of upper air over Jeju Island for 00:00 UTC on 25 February 2016

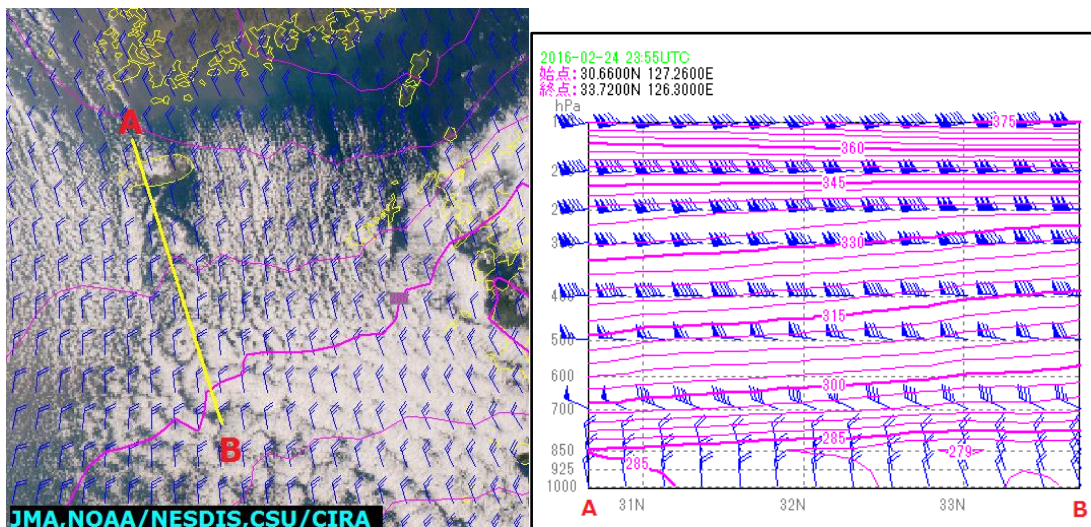


Fig. 3-18-4. True Color Reproduction image (left) and LFM (right) for 00:00 UTC on 25 February 2016; vertical section around Jeju Island for the same time period based on the initial value (a 925 hPa surface vertically sectioned at the yellow line); equivalent potential temperature (red lines) and wind (kt)

In the aerological vertical profile above Jeju Island (Fig. 3-18-3), a strong inversion layer is seen around 800 – 700 hPa with relatively high humidity around 800 hPa, providing a base for Sc cloud formation. Figure 3-18-4 shows a cross-section based on LFM in the vicinity of Karman vortices, indicating neutrality with no significant change in equivalent potential temperature under 800 hPa, and a dry stable layer above.

There is a significant uniform northern wind under 800 hPa without shears either in direction or wind speed. The environment satisfies the occurrence conditions as per Fig. 3-18-5.

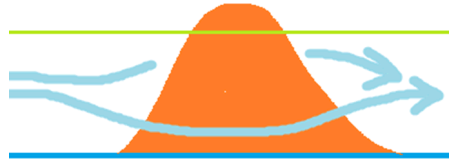


Fig. 3-18-5. Karman vortex emergence

The mountain top surpasses the inversion layer (green line), with wind detouring around the mass.

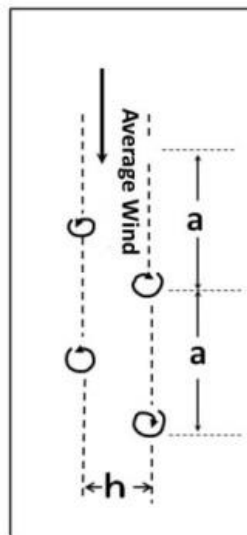


Fig. 3-18-6. Space **h** between vortex lines and space **a** between vortices in the line

Such conditions occur when air from the cold season gradually warms up, with Karman vortices running along lower-wind currents. They are frequently seen leeward of Jeju Island (1,950 m altitude), Yakushima Island (1,935 m) to the south, Rishiri Island (1,721 m), Urup Island (1,426 m) in the Kuril Islands, and Paramushir (1,816 m) to the north.

In satellite imagery (Fig. 3-18-2), a low cloud area with cold air is seen between the Yellow Sea and the East China Sea with prominent stratification around the Sakishima Islands. Two vortex lines (marked by arrows) appear, anticlockwise on the right and clockwise on the left, southward of Jeju Island. The ratio of the space **h** between the vortex lines and the space **a** between vortices in the line is expressed from a study by Chopra and Hubert (1965) as follows (Fig. 3-18-6):

$$0.28 < h/a < 0.52$$

Here, the vortices on the left and right are aligned with 3 – 4 turns each comprising Sc, with an **h/a** value of approximately 0.5.

Chapter 3. Cloud Patterns

The Reynolds number (Re) relating to Karman vortex generation is:

$$\text{Re} = U \cdot d/\nu$$

Here, U is natural fluid velocity, d is the obstacle diameter, ν is the molecular kinematic viscosity coefficient, and $\nu = \mu/\rho$ is the static viscosity coefficient of fluid divided by fluid density. Instead of applying the molecular kinematic viscosity coefficient, an eddy viscosity value of $107 \text{ cm}^2/\text{s}$ is used, with the diameter of Jeju Island as $30 \times 1,000 \text{ m}$ (the average diameter of the island's Hallasan volcano), wind speed as 10 m/s from aerological data, and Re as 300. Hence, Karman vortices on the leeward side of the mountain are in the range of $50 < \text{Re} < 300$ (from Science of Fluids, T. Kimura, 1979).

3.19. Belt-Form Convective Clouds

Numerous cloud streaks often appear along prominent winter winds over the Sea of Japan. These are typically seen in development from cloud streets reaching the Sanin district of Hokuriku in Japan from the edge of the Korean Peninsula. These are called belt-form convective clouds, and are closely related to heavy snowfall near the Sea of Japan. In the satellite imagery of Fig. 3-19-1, which corresponds to wind distribution around 925 hPa, a convergence zone of horizontal wind with strong horizontal shear is seen along the southwestern lining of the cloud band in the region enclosed with a broken line. This is known as the Japan Sea Polar air-mass Convergence Zone (JPCZ), considered to form under the influence of the range around South Korea's Mt. Paektu and the geographical distribution of land and sea (from *Meteorology of Heavy Rain and Snow*, Yoshizaki and Kato, 2007). Belt-form convective cloud is seen in response to the JPCZ.

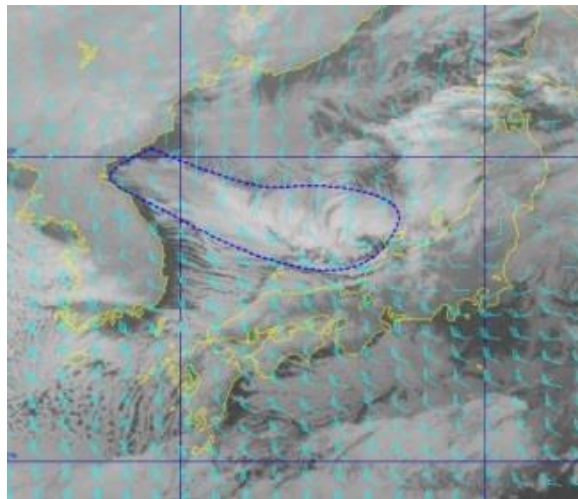


Fig. 3-19-1. B13 infrared image and MSM 925 hPa wind for 18:00 UTC on 23 January 2016

When belt-form convective cloud emerges, a synoptic scale trough tends to occur at the upper layer above Japan. A lower vortex (corresponding to a mesoscale cyclone, which in some cases develops into a synoptic-scale cyclone) may form within such cloud, causing heavy snowfall.

The process of belt-form convective cloud development and dissipation between 20 and 24 January 2016 is described below. Southern oscillation covering the entire formation was accompanied by a passing meso- α -scale trough (500 hPa), with a low vortex forming above the cloud in correspondence to a temperature trough (cold core: 700 hPa) behind the trough (MSC, 1992).

(1) Early Stage of Emergence

On a 500 hPa weather chart for 00:00 UTC on 20 January, the center of a cold low is seen over the sea east of Hokkaido, bringing a deep trough to the area around Japan and strong air influx below -30°C to the Sea of Japan (recorded as -36.7°C in Wajima). A strong wind axis

also passed from the area north of the Korean Peninsula and approached the Kii Peninsula (Fig. 3-19-2).

In satellite imagery, cloud streets are seen widely along with the cold air over the Sea of Japan, the Pacific and the East China Sea. No belt-form convective cloud is observed over the Sea of Japan, but cloud streets with a high top including Cg are seen moving toward Japan's Chugoku region. Also, at 925 hPa MSM, north-northwest flow fields are prominent around Japan, whilst a shear line (shown by the broken line in Fig. 3-19-3) formed over the east of the Korean Peninsula, corresponding to a high peak of equal potential temperature.

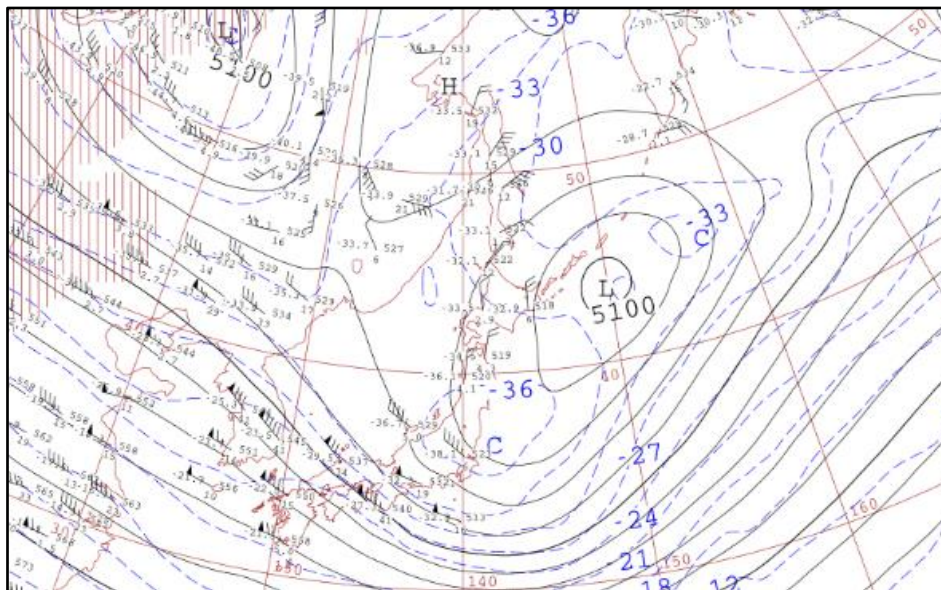


Fig. 3-19-2. 500 hPa weather chart for 00:00 UTC on 20 January 2016

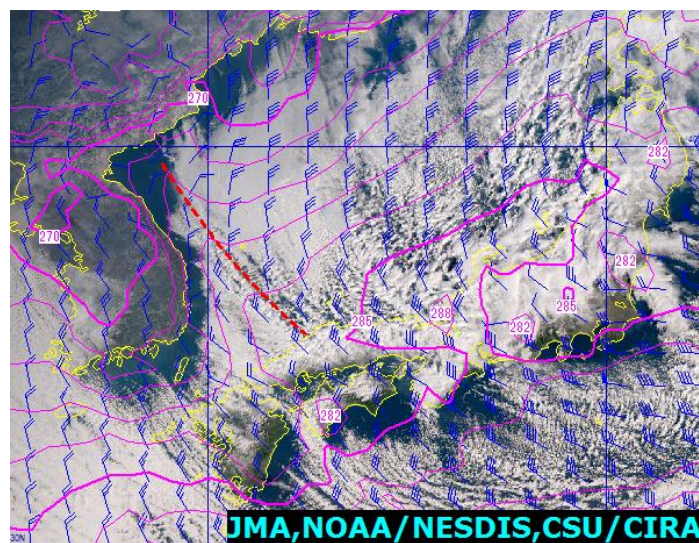


Fig. 3-19-3. True Color Reproduction image for 00:00 UTC on 20 January 2016 with equivalent potential temperatures and winds, MSM 925 hPa

(2) Development to Maturity

In satellite image for 21 January, a belt-form cloud band area is seen around lower shear over the Sea of Japan, with convective cloud containing Cg starting to develop to its west (Fig. 3-19-4).

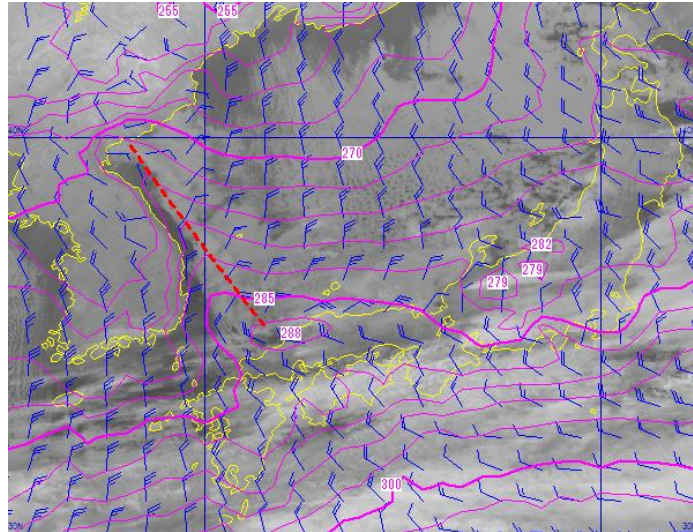


Fig. 3-19-4. B13 infrared image for 18:00 UTC on 21 January 2016 and equivalent potential temperature and wind, MSM 925 hPa

On the 500 hPa weather chart for 00:00 UTC on 23 January, a low with intense cold air under -45°C descended southward to around 41°N from Manchuria, bringing extremely cold air to the upper atmosphere toward western Japan. Short wave troughs around this cold low are observed over the western Sea of Japan and around the Yellow Sea (Fig. 3-19-5).

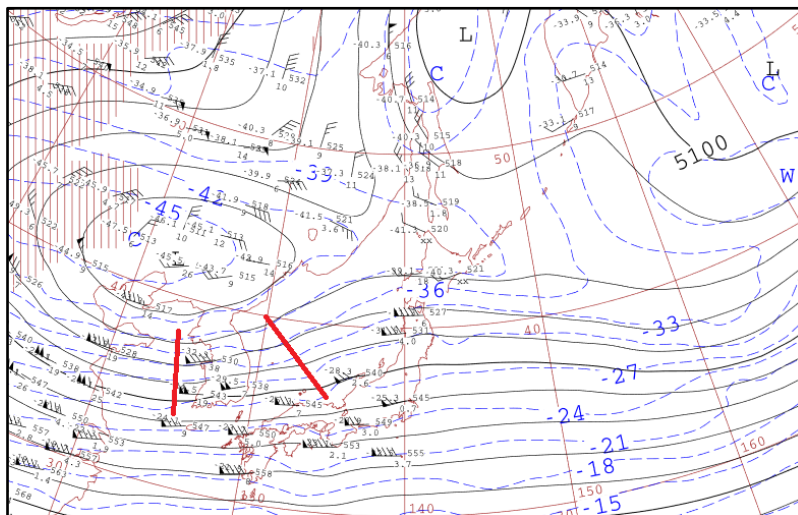


Fig. 3-19-5. 500 hPa weather chart for 00:00 UTC on 23 January 2016

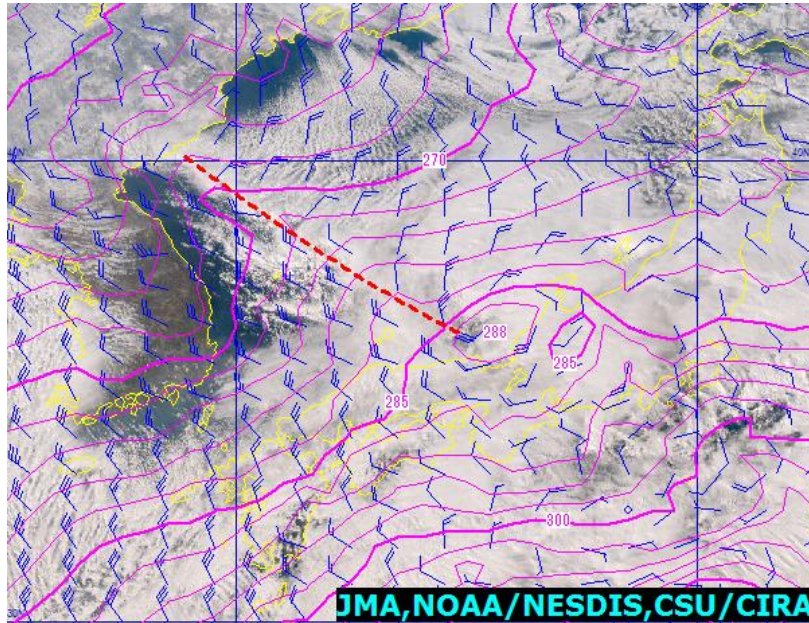


Fig. 3-19-6. True- Color Reproduction image with equivalent potential temperatures and wind, MSM 925 hPa for 06:00 UTC on 23 January 2016

The eastern edge of the belt-form convective clouds ascended northward alongside the current of a 500 hPa baroclinic zone toward the Hokuriku region. In the region indicated with a broken line in Fig. 3-19-6, north-northeast wind and northwest wind converge, with the highest cloud top at the south of the belt-form convective cloud, containing Cb and Cg, mixed with T-mode convective cloud. At the southern edge, a cloud vortex on a β -scale emerged, with a small cyclone observed around Wakasa Bay on the surface weather chart (Fig. 3-19-7). These belt-form convective clouds around minor cyclonic conditions are observed migrating toward Japan's Hokuriku district.

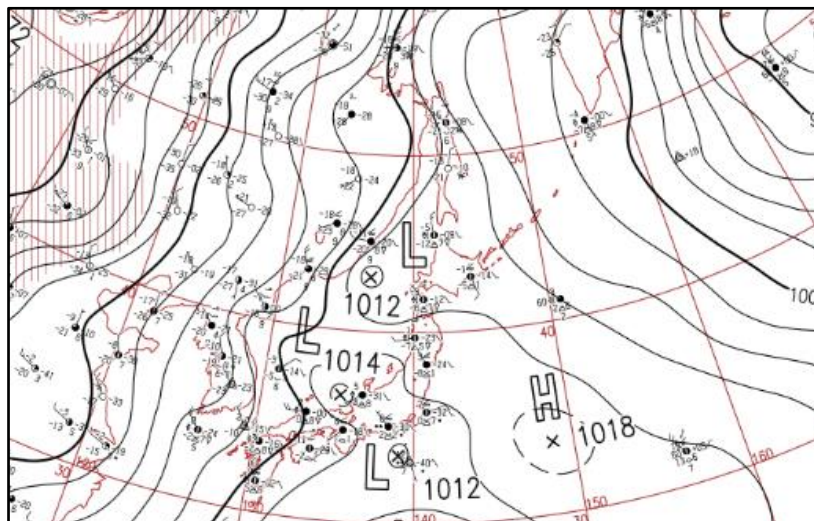


Fig. 3-19-7. Surface weather chart for 06:00 UTC on 23 January 2016

(3) Dissipation Stage

On the 500 hPa weather chart for 00:00 UTC on 24 January, a low above northeastern

China is seen descending southward to the Sea of Japan with air at -42°C at its center. The trough is latitudinal over western Japan with a strong wind axis descending south toward the Pacific coast, bringing a flow field between western and west-southwestern Japan (Fig. 3-19-8).

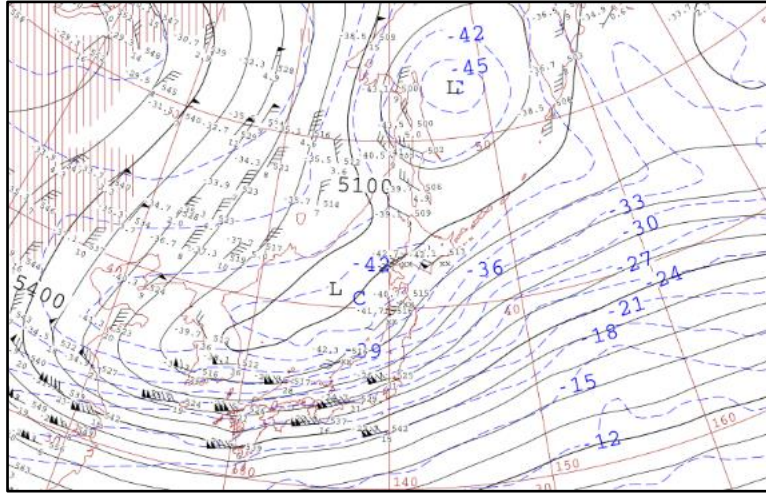


Fig. 3-19-8. 500 hPa weather chart for 00:00 UTC on 24 January 2016

In the corresponding satellite imagery (Fig. 3-19-9), belt-form convective cloud is seen descending southward along lower-layer shear at 925 hPa with a latitudinal strike. A lower eddy made landfall on the Hokuriku district and then disappeared. At 12:00 UTC on the same day, the belt-form convective cloud descended further south to the Sea of Japan coast with Cg and Cb (Fig. 3-19-10). In the Cb region, snowfall of over 10 cm was observed within the space of an hour. After making landfall, the formation dissipated with gradually descending cloud top heights and did not cross Japan's backbone mountain range. Cloud streets were prominent at the north of the formation, resulting in a strong winter-type pressure pattern.

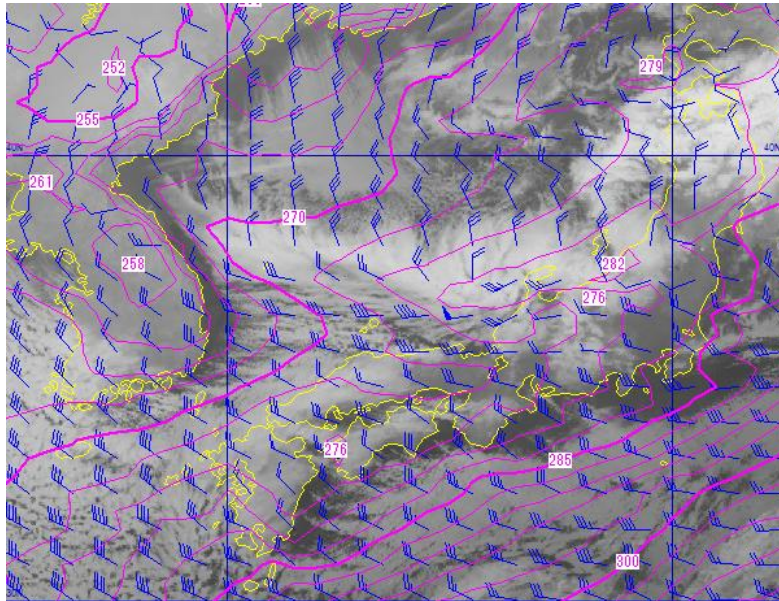


Fig. 3-19-9. B13 infrared image for 00:00 UTC on 24 January 2016 and equivalent potential temperatures and winds, MSM 925 hPa

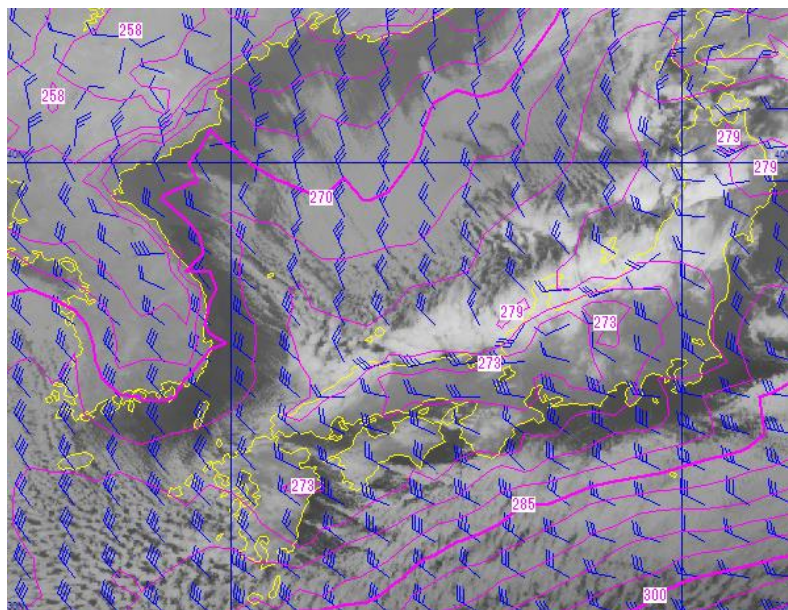


Fig. 3-19-10. B13 infrared image for 12:00 UTC on 24 January 2016 and equivalent potential temperatures and winds, MSM 925 hPa

Below is a summary of the changes and movements of the belt-form convective cloud provided in this example.

- Belt-form convective cloud emerged at the lower shear part over the western Sea of Japan with gradually rising top height, forming a band extending southeastward.
- The cloud position showed a parallel tendency to a large scale stream, changing direction along with localized streams depending on progressive short-wave phases with temporal

and spatial developments.

- The cloud form was at its least stable under short wave trough conditions with maximum air mass change and then developed significantly, in some cases displaying meso- β -scale lower-eddy conditions above nearby trough areas.
- The cloud exhibited latitudinal strike conditions along the movement of cold low and trough areas, and dissipated after making landfall between the Sanin and Hokuriku districts. In both areas, snowfall intensified after landfall.

In other cases of dissipation, belt-form convective cloud is weakened and disappears with decreased air-mass modification over sea areas when tropospheric conditions are stable due to the passage of troughs that raise density over the Sea of Japan.

3.20. Ship Trails

Over sea areas with lower clouds, stratocumulus cloud streets with widths of 10 – 30 km and lengths of up to 1,000 km may form. These are called ship trails for their close association with shipping operations, and are a man-made phenomenon. Ship trails often form around July with a high frequency of sea fog, resulting in multiple cloud streaks lasting for several days (Takasaki, 1984). The main cause of ship trails is flue gas generated by ships operating along particular passages, forming small cloud particle nuclei that generate denser cloud than natural stratocumulus over the sea. They exhibit higher brightness than surrounding clouds in visible and near-infrared image, but are harder to identify in infrared image (Band 13) because of their lower cloud top. Ship trails can also be identified in particular time zones with sunlight via Band 7 data or differences between Band 7 and Band 13 image.

The visible imagery (Band 3) in Fig. 30-20-1 shows ship trails. Several cloud streaks with lengths of around 100 km are seen eastward from around 200 km over the sea to the east of the Kamchatka Peninsula. In the center of the figure around Attu Island (circled), ship trail deformation is seen due to the geographical effects of the terrain. In Natural Color RGB composite image, ship trails can be identified through upper-layer clouds in semi-transparent cyan in the areas around the red ovals in Fig. 3-20-2.

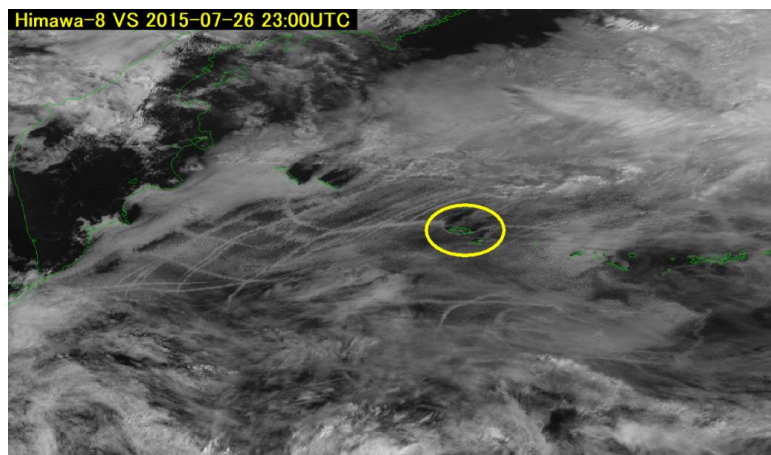


Fig. 3-20-1. B03 visible image of ship trails for 23:00 UTC on 26 July 2015

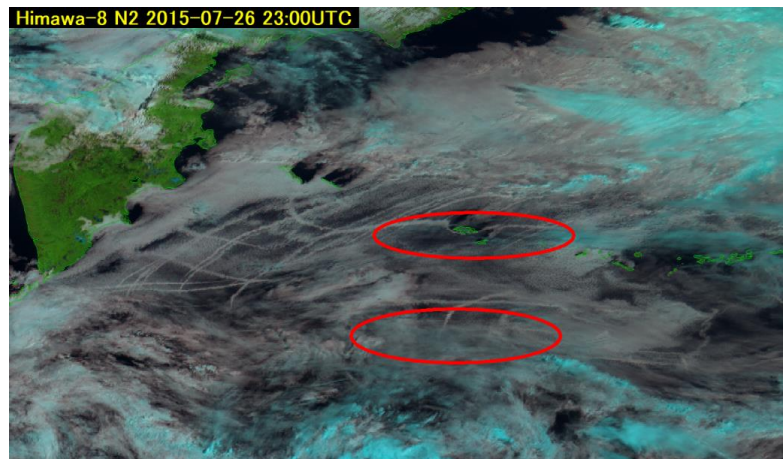


Fig. 3-20-2. Natural-Color RGB composite image of ship trails for 23:00 UTC on 26 July 2015

Reference:

- Maddox, R. A., 1980: Mesoscale Convective Complexes, *Bull. Amer. Met. Soc.*, 61, 1374 - 1387.
- Iwasaki, H and Takeda T.,1993: Characteristic features on meso-scale cloud clusters around Japan in the Baiu-season from 1985 to 1988, *Tenki*, 40, 3, 161 – 170 (in Japanese)
- Shimizu K. and Tsuboki K., 2004: Observational study on the process of transverse-type snowfall band formation; Hydrospheric Atmospheric Research Center (HyARC), Nagoya University; Snow and Ice Research Center, National Research Institute for Earth Science and Disaster Resilience (in Japanese)
- Yagi S., 1985: Large scale snow clouds with roll axes roughly perpendicular to the direction of winter monsoon burst: observational studies of convective cloud roll axes and some theoretical consideration, *Tenki*, 32,4, 175-187 (in Japanese).
- Takasaki H., 1984: Peculiar cloud streets in the north pacific region, *Tenki*, 31, 5, 315-318 (in Japanese)

